Gluon mass scale through nonlinearities and vertex interplay

A. C. Aguilar[1], M. N. Ferreira[1,2], C. T. Figueiredo[1,2] and J. Papavassiliou[2]

[1]*University of Campinas—UNICAMP, Institute of Physics "Gleb Wataghin",*
13083-859 Campinas, SP, Brazil
[2]*Department of Theoretical Physics and IFIC, University of Valencia and CSIC, E-46100, Valencia, Spain*

We present a novel analysis of the gluon gap equation, where its full nonlinear structure is duly taken into account. In particular, while in previous treatments the linearization of this homogeneous integral equation introduced an indeterminacy in the scale of the corresponding mass, the current approach determines it uniquely, once the value of the gauge coupling at a given renormalization point is used as input. A crucial ingredient for this construction is the "kinetic term" of the gluon propagator, whose form is not obtained from the complicated equation governing its evolution, but is rather approximated by suitable initial *Ansätze*, which are subsequently improved by means of a systematic iterative procedure. The multiplicative renormalization of the central equation is carried out following an approximate method, which is extensively employed in the studies of the standard quark gap equation. This approach amounts to the effective substitution of the vertex renormalization constants by kinematically simplified form factors of the three- and four-gluon vertices. The resulting numerical interplay, exemplified by the infrared suppression of the three-gluon vertex and the mild enhancement of the four-gluon vertex, is instrumental for obtaining positive-definite and monotonically decreasing running gluon masses. The resulting gluon propagators, put together from the gluon masses and kinetic terms obtained with this method, match rather accurately the data obtained from large-volume lattice simulations.

I. INTRODUCTION

The nonperturbative aspects of the gluon propagator, both in pure Yang-Mills theory and in QCD, are believed to be relevant for our understanding of a wide range of important physical phenomena, such as the dynamical generation of a mass gap, confinement, chiral symmetry breaking, and the formation of bound states such as mesons, baryons, glueballs, hybrids, and exotics [1–17]. A particularly interesting feature of the gluon propagator, which manifests itself both in the Landau gauge and away from it, is the saturation of its scalar form factor, $\Delta(q^2)$, in the deep infrared, i.e., $\Delta(0) = c > 0$. This special behavior, which is intimately connected with the emergence of a gluon mass scale [18–24], has been firmly established in a variety of SU(2) [25–28] and SU(3) [29–34] large-volume lattice simulations, and has been extensively studied in the continuum within diverse theoretical frameworks [35–55].

One of the approaches put forth in order to explain the infrared saturation of $\Delta(q)$ relies on the implementation of the Schwinger mechanism [56,57] at the level of the Schwinger-Dyson equation (SDE) that controls the momentum evolution of $\Delta(q)$. This SDE, in turn, has been formulated within the framework developed through the merging of the pinch-technique (PT) [7,18,58,59] with the background-field method (BFM) [60–64], known as the "PT-BFM scheme" [36,65]. $\Delta(q)$ is subsequently written as the sum of two distinct components, the kinetic term, $J(q)$, and the mass term, $m^2(q)$, according to Eq. (2.2). This splitting enforces a special realization of the Slavnov-Taylor identity (STI) satisfied by the fully dressed three-gluon vertex entering in the gluon SDE [see Eq. (2.7)], leading finally to the separation of this dynamical equation into a a system of two coupled integral equations, one for each component [66].

Even though the derivation of the aforementioned system is theoretically well-defined, its complete treatment is still pending, mainly due to the technical complexities associated with the equation governing $J(q)$. Instead, one considers only the homogeneous integral equation for $m^2(q)$, whose form is given by

$$m^2(q) = \int_k m^2(k)\Delta(k)\Delta(k+q)\mathcal{K}(k, q, \alpha_s), \quad (1.1)$$

and solves it in isolation [66,67]; the precise definition of the integration $\int_k$ is given in Eq. (2.11), and $\alpha_s := g^2/4\pi$,

where g denotes the gauge coupling. In particular, the propagators Δ appearing in Eq. (1.1) are *not* decomposed according to Eq. (2.2) but are rather treated as *external* quantities, whose form is taken from the data of large-volume lattice simulations. This practical simplification, however, distorts the true nature of the original equation, converting it to a *linear* integral equation. As a consequence, one has to deal with an eigenvalue problem, which has a solution for a *unique* value of α_s, rather than a continuous interval of values. Moreover, due to its linearity, the equation admits a family of solutions parametrized by a real constant $c_0 > 0$, since, if $m^2(q)$ is a solution, so is $c_0 \times m^2(q)$ (for that unique α_s). This fact, in turn, introduces an ambiguity in the physics, because the final scale must be introduced "by hand," with no clear connection to the fundamental parameters of the theory.

Evidently, it would be far preferable to work with a dynamical equation that allows one to determine how the emergent scale responds to changes in the value of α_s at a given scale μ, furnishing the "correct" mass (i.e., the one set by the lattice) once a special value for α_s has been chosen. In that sense, one is seeking to replicate the circumstances that occur in the context of the quark gap equation, where α_s may be varied, within a reasonable range, giving rise to a continuous set of quark masses; and once the value of the quark mass has been fixed with a given accuracy (say, from the lattice), a firm restriction on the allowed values for α_s may be obtained. As we will show in the present work, this is indeed what happens after the nonlinear nature of the original gluon mass equation has been restored.

In practice, the restoration of the nonlinearity of Eq. (1.1) is accomplished by implementing in it the substitution Eq. (2.2), using a set of physically motivated *Ansätze* for $J(q)$. Specifically, even in the absence of a full treatment of the corresponding dynamical equation, the preeminent qualitative features of $J(q)$ are relatively well known, due to its profound relation with the three-gluon vertex [68,69]. In particular, as the Euclidean momentum q^2 decreases, $J(q)$ departs gradually from its tree-level value, reverses its sign ("zero-crossing"), and finally diverges logarithmically at the origin. In fact, as has been argued in the works cited above, these special properties of $J(q)$ are inextricably connected with the infrared suppression displayed by the main form factors of the three-gluon vertex [70–79]. When a $J(q)$ that encodes the above features is used as an initial "seed," and a value for α_s is chosen, the gluon mass equation yields a unique $m^2(q)$. The procedure is further refined by modifying the shape of $J(q)$ and by adjusting[1] the value of α_s, such that the resulting propagator, obtained by combining $J(q)$ and $m^2(q)$ according to Eq. (2.2), matches the lattice result as accurately as possible.

There is an additional issue that appears when dealing with the gluon mass equation (1.1), related with the relative

size of the one-loop and two-loop dressed contributions, which enter in the kernel $\mathcal{K}(k, q, \alpha_s)$ with a relative minus sign. Specifically, a positive-definite and monotonically decreasing solution for $m^2(q)$ requires a delicate balance between these two terms, which depends, among other things, on the way that the multiplicative renormalization of the equation is enforced. In the case of the quark gap equation, this problem has been dealt with by means of an approximate method, which amounts to the substitution of the renormalization constants by appropriately chosen momentum-dependent functions [17,80–82]. In this work we resort to the same expedient, appropriately adapted to the specific vertices appearing in the problem. It turns out that its implementation introduces a subtle interplay between the three- and four-gluon vertices, which is instrumental for the overall stability of the resulting integral equation.

The article is organized as follows. In Sec. II we review the most salient features of the integral equation that governs the existence and momentum evolution of $m^2(q^2)$. Then, in Sec. III we present the procedure adopted for the effective implementation of the multiplicative renormalization, drawing an analogy with the more familiar case of the quark gap equation, and elaborating on the main underlying assumptions. In Sec. IV we discuss in detail the origin and properties of the various ingredients entering in the kernel of the gluon mass equation. In Sec. V we present a thorough numerical study of the resulting integral equation, and obtain solutions for $m^2(q^2)$ that reproduce quite accurately the saturation scale of the gluon propagator observed in lattice simulations, for values of α_s that are in accordance with the theoretical expectations. Finally, in Sec. VI we discuss our results and comment on further possible directions.

II. GLUON MASS EQUATION: A BRIEF OVERVIEW

In this section we briefly review the structure of the gluon mass equation, and discuss in some detail its multiplicative renormalization.

A. Basic concepts and ingredients

Throughout this article we work in the *Landau gauge*, where the gluon propagator $\Delta_{\mu\nu}^{ab}(q) = -i\delta^{ab}\Delta_{\mu\nu}(q)$ is completely transverse, given by

$$\Delta_{\mu\nu}(q) = \Delta(q)\mathrm{P}_{\mu\nu}(q), \qquad \mathrm{P}_{\mu\nu}(q) = g_{\mu\nu} - \frac{q_\mu q_\nu}{q^2}. \quad (2.1)$$

The special property of infrared saturation displayed by $\Delta(q)$ prompts its splitting into two separate components, according to (Euclidean space) [66]

$$\Delta^{-1}(q) = q^2 J(q) + m^2(q), \qquad (2.2)$$

---

[1]As we will see in Sec. V, a precision of about 1% is required.
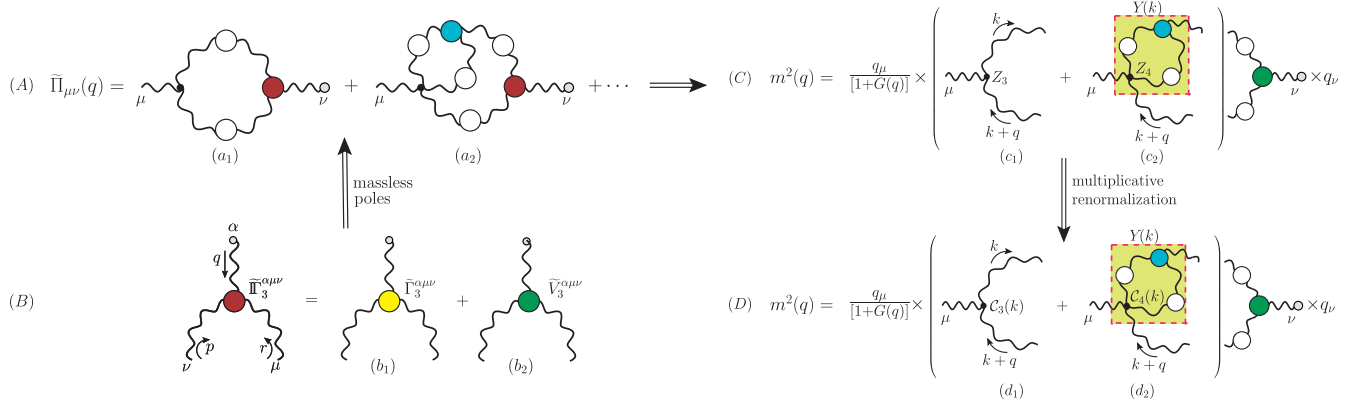
FIG. 1.   The schematic representation of the steps involved in the derivation of the dynamical gluon mass equation in the PT-BFM framework. White (colored) circles denote fully dressed propagators (vertices).

where $J(q)$ corresponds to the so-called "kinetic term" (at tree-level, $J(q) = 1$), while $m^2(q)$ to a momentum-dependent gluon mass scale, with the property $m^2(0) = \Delta^{-1}(0)$. For large values of q^2, the component $J(q)$ captures standard perturbative corrections to the gluon propagator, while in the infrared it exhibits several exceptional characteristics [68,69].

The full dynamical evolution of the functions $J(q)$ and $m^2(q)$ is determined by two separate, but coupled, integral equations, whose derivation may be carried out within the PT-BFM framework [36,65,83]. To that end, the most advantageous starting point is the mixed propagator connecting a quantum (Q) and a background (B) gluon, to be denoted by $\tilde{\Delta}(q^2)$; the diagrammatic representation of its self-energy, $\tilde{\Pi}_{\mu\nu}(q)$, is given in panel (A) of Fig. 1. When contracted by the momentum q^ν, the fully dressed vertices appearing in $\tilde{\Pi}_{\mu\nu}(q)$ satisfy Abelian STIs; for instance, the BQQ vertex appearing in the panel (B) of Fig. 1 satisfies

$$q_\alpha \tilde{\mathbf{\Gamma}}_3^{\alpha\mu\nu}(q, r, p) = \Delta^{-1}(p)\mathrm{P}^{\mu\nu}(p) - \Delta^{-1}(r)\mathrm{P}^{\mu\nu}(r). \quad (2.3)$$

This property, in turn, makes the realization of the transversality condition $q^\nu \tilde{\Pi}_{\mu\nu}(q) = 0$ considerably more transparent. Note also that the conventional (QQ) gluon propagator, $\Delta(q^2)$, is connected to $\tilde{\Delta}(q^2)$ by the exact relation [84,85],

$$\Delta(q) = [1 + G(q)]\tilde{\Delta}(q), \quad (2.4)$$

where $1 + G(q)$ is the $g_{\mu\nu}$ cofactor of a special two-point correlation function (see [86] and references therein), intrinsic to the Batalin-Vilkovisky formalism. Thus, the SDE of interest reads

$$[q^2 J(q) + m^2(q)]\mathrm{P}_{\mu\nu}(q) = \frac{q^2 \mathrm{P}_{\mu\nu}(q) + i\tilde{\Pi}_{\mu\nu}(q)}{1 + G(q^2)}. \quad (2.5)$$

As has been explained in detail in a series of works (see, e.g., [87,88]) the emergence of an infrared finite solution for Δ proceeds through the activation of the *Schwinger mechanism* by *longitudinally coupled massless poles* contained in the vertex $\tilde{\mathbf{\Gamma}}_3$ [56,57,89–92]. Specifically, one separates the three-gluon vertex $\tilde{\mathbf{\Gamma}}_3$ into two distinct parts,

$$\tilde{\mathbf{\Gamma}}_3^{\alpha\mu\nu}(q, r, p) = \tilde{\Gamma}_3^{\alpha\mu\nu}(q, r, p) + \tilde{V}_3^{\alpha\mu\nu}(q, r, p), \quad (2.6)$$

where $\tilde{\Gamma}_3$ is polefree,[2] while $\tilde{V}_3^{\alpha\mu\nu}(q, r, p)$ denotes the part containing the massless bound-state excitations [87] [see panel (B) in Fig. 1]. These two components of the full vertex contribute to the realization of Eq. (2.3) in a very particular way: when the terms Δ^{-1} on the r.h.s. of Eq. (2.3) are written in the form of Eq. (2.2), then the divergence of $\tilde{\Gamma}_3$ on the l.h.s. accounts for the appearance of the J terms, while $\tilde{V}_3$ for the masses, i.e.,

$$q_\alpha \tilde{\Gamma}_3^{\alpha\mu\nu}(q, r, p) = p^2 J(p)\mathrm{P}^{\mu\nu}(p) - r^2 J(r)\mathrm{P}^{\mu\nu}(r),$$
$$q_\alpha \tilde{V}_3^{\alpha\mu\nu}(q, r, p) = m^2(p)\mathrm{P}^{\mu\nu}(p) - m^2(r)\mathrm{P}^{\mu\nu}(r). \quad (2.7)$$

From this point on, the derivation of the equations for $m^2(q)$ and $J(q)$ proceeds by associating the pole related parts of each diagram on the r.h.s. of Eq. (2.5) with the $m^2(q)$ term on the l.h.s., assigning the remaining pieces to the equation for $J(q)$ [see panel (C) in Fig. 1]. Focusing on the former case, after certain algebraic manipulations [66], the integral equation that controls the evolution of $m^2(q)$ is given by

$$m^2(q) = \frac{g^2 C_A}{1 + G(q)} \frac{1}{q^2} \int_k m^2(k)\Delta(k)\Delta(k + q)\mathcal{K}_m(q, k), \quad (2.8)$$

---

[2]Note, however, that it contains logarithmic infrared divergences [68,69].

where C_A represents the Casimir eigenvalue of the adjoint representation [N for SU(N)], the kernel $\mathcal{K}_m(q,k)$ is given by

$$\mathcal{K}_m(q,k) = \{\mathcal{K}^+(q,k)[(k+q)^2 - k^2]g^{\alpha\beta} + \mathcal{K}^-(q,k)(q^2 g^{\alpha\beta} - 2q^\alpha q^\beta)\}\mathrm{P}^\rho_\alpha(k)\mathrm{P}_{\beta\rho}(k+q), \quad (2.9)$$

with

$$\mathcal{K}^+(q,k) = [Y(k+q) + Y(k)] - 1,$$
$$\mathcal{K}^-(q,k) = [Y(k+q) - Y(k)], \quad (2.10)$$

and we have defined

$$\int_k := \int \frac{\mathrm{d}^4 k}{(2\pi)^4}. \quad (2.11)$$

Finally, the function $Y(k)$ originates from the subgraph shown in the two-loop diagram (c_2) of Fig. 1; its closed expression is given in Eq. (4.9).

B. Renormalization of the gluon mass equation

At the formal level, the renormalization of Eq. (2.8) is carried out multiplicatively, through the introduction of the appropriate wave function, vertex, and gauge coupling renormalization constants. Specifically, the fully dressed renormalized quantities (carrying the index "R") are related to the bare ones through [67]

$$\Delta_R(q) = Z_A^{-1}\Delta(q),$$
$$1 + G_R(q) = Z_G[1 + G(q)],$$
$$\Gamma_{3R}^{\mu\alpha\beta}(q,r,p) = Z_3\Gamma_3^{\mu\alpha\beta}(q,r,p),$$
$$g_R = Z_g^{-1}g, \quad (2.12)$$

where all renormalization constants Z_i depend both on the ultraviolet cutoff and the renormalization point μ. In what follows we employ the momentum subtraction (MOM) scheme [93,94]; propagators assume their tree-level values at the subtraction point μ, while an analogous condition is imposed on the vertices at special momentum configurations, such as the "symmetric" point.

Then, the renormalization of Eq. (2.8) is carried out by replacing the bare quantities appearing in them by their renormalized counterparts, according to Eq. (2.12). Specifically, suppressing all momentum arguments and indices, omitting the integral signs $\int_k$ and $\int_\ell$, and setting $Y \sim g^2\Delta^2\Gamma_3$ [see Eq. (4.9)], we have

$$g^2\Delta^2[1+G]^{-1} = Z_3 g_R^2\Delta_R^2[1+G_R]^{-1},$$
$$g^4\Delta^4\Gamma_3[1+G]^{-1} = Z_4 g_R^4\Delta_R^4\Gamma_{3R}[1+G_R]^{-1}. \quad (2.13)$$

In deriving the above results we have used the crucial constraints that the fundamental STIs of the theory impose on the renormalization constants, namely

$$Z_g = Z_3 Z_A^{-3/2} = Z_G^{-1}Z_A^{-1/2} = Z_4^{1/2}Z_A^{-1}, \quad (2.14)$$

where the last relation involves the four-gluon vertex renormalization constant, Z_4, defined as (suppressing color indices)

$$\Gamma_{4R}^{\mu\nu\rho\sigma}(q,r,p,t) = Z_4\Gamma_4^{\mu\nu\rho\sigma}(q,r,p,t). \quad (2.15)$$

Note that (i) the fully dressed vertex $\Gamma_{\mu\nu\rho\sigma}(q,r,p,t)$ does *not* appear in Eq. (2.8); only its tree-level version, $\Gamma_{\mu\nu\rho\sigma}^{(0)}$, appears in graph ($c_2$) of Fig. 1, and (ii) the second relation of Eq. (2.14) originates from the fact that, due to the special properties of the PT-BFM framework, the combination [49,86,95]

$$\mathcal{R}_G = g\Delta^{1/2}(q)[1+G(q)]^{-1} = g_R\Delta_R^{1/2}(q)[1+G_R(q)]^{-1}, \quad (2.16)$$

is renormalization-group invariant (RGI) [independent of the choice of the renormalization (subtraction) scale μ, and the ultraviolet cutoff Λ].

Armed with the above relations, it is relatively straightforward to establish that the net effect of renormalization amounts to the replacement of bare by renormalized quantities on both sides of Eq. (2.8), together with the modification of the kernels of Eq. (2.10) into

$$\mathcal{K}_R^+(q,k) = Z_4[Y_R(k+q) + Y_R(k)] - Z_3,$$
$$\mathcal{K}_R^-(q,k) = Z_4[Y_R(k+q) - Y_R(k)], \quad (2.17)$$

as illustrated in panel (C) of Fig. 1.

III. EFFECTIVE TREATMENT OF MULTIPLICATIVE RENORMALIZATION

The rigorous implementation of multiplicative renormalization at the level of SDEs is known to be an exceptionally complicated issue, which, at the practical level, is resolved by means of certain approximate approaches (see, e.g., [96,97]). In this section we present an effective treatment of this problem, whose origin may be traced back to analogous approaches implemented in the studies of the quark gap equation [80–82] and the SDEs of vertices [17]. The upshot of this analysis is that the constants Z_3 and Z_4 in Eq. (2.17) will be replaced by appropriate form factors of the three- and four-gluon vertices, respectively.

A. The quark gap equation paradigm

It is clear that the Z_3 and Z_4 survive in the final answer because the three- and four-gluon vertices carrying the index μ, in the diagrams (c_1) and (c_2) of Fig. 1, are bare instead of fully dressed. In fact, this is completely analogous to what happens in the more familiar case of the quark gap equation, where, by the end of the renormalization
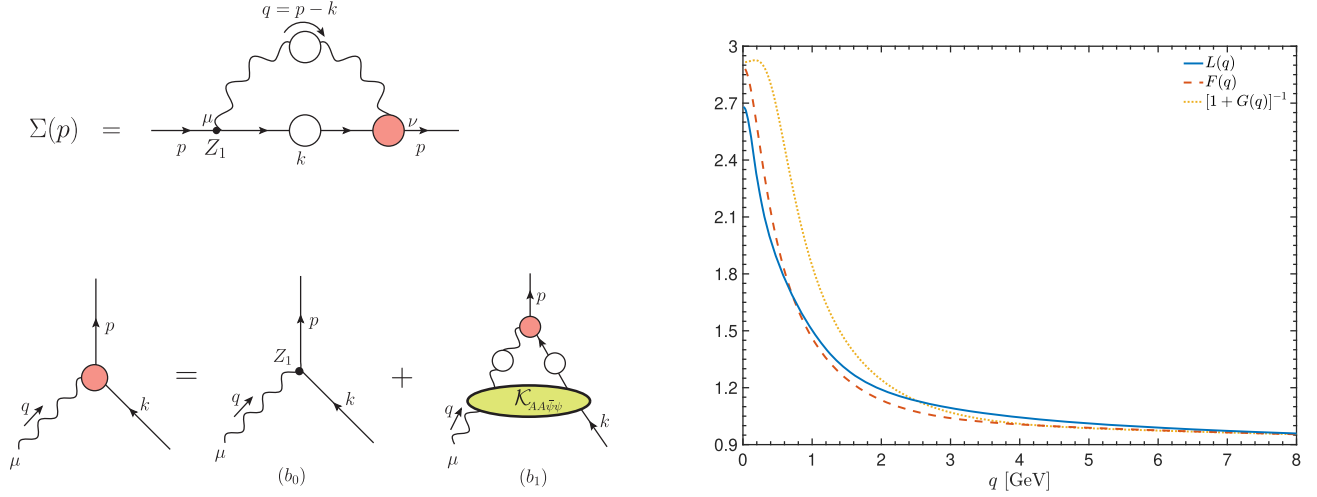
FIG. 2. Left panel: The quark gap equation (top) and the SDE for the quark-gluon vertex Γ^μ (bottom), expressed with the quark providing the "reference" leg [98]. Right panel: The three versions of $\mathcal{C}_1(q)$ listed in Eq. (3.10).

procedure, the quark self-energy is multiplied by the renormalization constant Z_1 of the quark-gluon vertex, as shown in the top panel of Fig. 2.

To illustrate this correspondence in some detail, recall that the inverse of the full quark propagator can be written as $S^{-1}(p) = A(p)\not{p} - B(p)\mathbb{I}$, and the dynamical quark mass function is given by $\mathcal{M}(p) = B(p)/A(p)$. In the absence of a current quark mass (chiral limit), after the implementation of certain simplifying assumptions that do not compromise the features we want to examine, the quark mass equation may be brought to the form [81]

$$\mathcal{M}(p) = cg_R^2 Z_1 \int_k \text{Tr}[\Gamma_\mu^{(0)} S_R(k) \Gamma_\nu^R(-p,k,q) \Delta_R^{\mu\nu}(q)],$$

(3.1)

where c is a numerical constant, the trace runs over spinor indices,[3] $q = p - k$, and $\Gamma_\nu(-p,k,q)$ denotes the fully dressed quark-gluon vertex, whose tree-level value is given by $\Gamma_\nu^{(0)} = \gamma_\nu$. To arrive at Eq. (3.1), one employs the first and fourth relations in Eq. (2.12), together with

$$S_R(p) = Z_f^{-1} S(p), \qquad \Gamma_\nu^R(-p,k,q) = Z_1 \Gamma_\nu(-p,k,q),$$
$$Z_g^{-1} = Z_1^{-1} Z_f Z_A^{1/2}.$$

(3.2)

The next step is to write the kernel of Eq. (3.1) in terms of a manifestly RGI quantity multiplied by a momentum- and μ-dependent remainder. To that end, and in order to simplify the discussion, we retain only one out of the twelve tensorial structures comprising $\Gamma_\nu^R(-p,k,q)$ [99], namely the one proportional to its tree-level tensor, $\Gamma_\nu^{(0)}$.

Moreover, the form factor multiplying $\Gamma_\nu^{(0)}$, denoted by $L_R(-p,k,q)$, will be evaluated in the so-called *symmetric configuration*, where $p^2 = k^2 = q^2$, thus becoming a function of a single momentum [82], i.e.,

$$\Gamma_\nu^R(-p,k,q) \to L_R(q)\Gamma_\nu^{(0)}(-p,k,q).$$

(3.3)

At this point it is convenient to introduce the standard RGI quantity

$$\mathcal{R}_f(q,r,p) = g\Delta^{1/2}(q)S^{1/2}(r)S^{1/2}(p)L(q),$$

(3.4)

which finally allows one to cast Eq. (3.1) into the alternative form[4]

$$\mathcal{M}(p) = cZ_1 \int_k L_R^{-1}(q)\text{Tr}[\Gamma_\mu^{(0)}\mathcal{R}_f^2 \Gamma_\nu^{(0)} \mathsf{P}^{\mu\nu}(q)]\mathcal{M}(k),$$

(3.5)

which is the announced result.[5]

Given that $\mathcal{M}(p)$ is RGI, i.e., $d\mathcal{M}(p)/d\mu = 0$, the r.h.s. of Eq. (3.5) must display the same property; then, since $\mathcal{R}_f^2$ is RGI by itself, one must have that $d[Z_1 L_R^{-1}(q)]/d\mu = 0$. This is indeed true, because, from the second relation in Eq. (3.2) and Eq. (3.3), we have $Z_1 L_R^{-1}(q) = L^{-1}(q)$, and, since $L(q)$ is a bare quantity, it is trivially μ-independent, $dL(q)/d\mu = 0$. Therefore, at this point it is clear that

---

[3] The application of the trace on both sides of the gap equation isolates the term $B(p)$.

[4] The trace may be carried out trivially; however, for the arguments that follow, it is advantageous to retain the vertices $\Gamma^{(0)}$ manifestly in the integrand.

[5] Note that the ratio $H(p_1)/H(p_2)$ of any two-point function $H(p)$ is also a RGI quantity; this fact may be used in order to "compensate" for "mismatches" of momenta when forming RGI products. Such factors are immaterial for the discussion that follows and will be omitted throughout.

setting $Z_1 = 1$ would distort the RG properties of the r.h.s. of Eq. (3.1).

Evidently, the simplest way to enforce the relation $d[Z_1 L_R^{-1}(q)]/d\mu = 0$ would be to carry out the replacement $Z_1 L_R^{-1}(q) \to \mathcal{R}$, where $\mathcal{R}$ is some RGI combination. In fact, the most obvious "solution" would be to simply set $\mathcal{R} = 1$, which, interestingly enough, is precisely the one needed for recovering the correct one-loop anomalous dimension of $\mathcal{M}(p)$ [81,82]. Thus, effectively, one implements the substitution $Z_1 \to L_R(q)$ into Eq. (3.5), i.e.,

$$\mathcal{M}(p) = c \int_k \mathrm{Tr}[\Gamma_\mu^{(0)} \mathcal{R}_f^2 \Gamma_\nu^{(0)} \mathrm{P}^{\mu\nu}(q)] \mathcal{M}(k). \quad (3.6)$$

Clearly, due to its RGI nature, $\mathcal{M}(p)$ does not depend on the subtraction point μ nor on the ultraviolet cutoff Λ, i.e., $d\mathcal{M}(p)/d\Lambda = 0$. Consequently, the implicit Λ-dependence of the integral on the r.h.s. of Eq. (3.1) or Eq. (3.5) should be canceled by the corresponding Λ-dependence of Z_1. Of course, the operation $Z_1 \to L_R(q)$ implemented above amounts to replacing a Λ-dependent constant by a Λ-independent (but μ-dependent) function of q^2, which, in principle, could distort the aforementioned cancellation. Therefore, the underlying assumption when carrying out this substitution is that the introduction of $L_R(q)$ in the integrand of Eq. (3.1) or Eq. (3.5) will alter the initial Λ-dependence of the integral in such a way that, as $\Lambda \to \infty$, the resulting solution will satisfy the condition $d\mathcal{M}(p)/d\Lambda = 0$. As we will check explicitly in Sec. V B, this is indeed what happens in the case of the gluon mass equation.

B. The SDE of the quark-gluon vertex: "Solving" for Z_1

The above heuristic substitution $Z_1 \to L_R(q)$ admits a simple interpretation in the context of the SDE satisfied by the quark-gluon vertex Γ^μ, being essentially an application of the so-called *dressed skeleton expansion* [100] (for recent treatments see, e.g., [101–103]).

In particular, let us consider the SDE for Γ^μ, which, when set up from the point of view of the quark leg [98] contains a single dressed contribution, shown by the diagram (b_1) in Fig 2. Its main ingredient is the amputated 4-point kernel with two gluons and a quark-antiquark pair entering in it, denoted by $\mathcal{K}_{AA\bar\psi\psi}$, which is related to its renormalized counterpart, $\mathcal{K}_{AA\bar\psi\psi}^R$, by $\mathcal{K}_{AA\bar\psi\psi}^R = Z_A Z_f \mathcal{K}_{AA\bar\psi\psi}$. Clearly, the combination $\hat{\mathcal{K}}_{AA\bar\psi\psi} = \Delta S \mathcal{K}_{AA\bar\psi\psi}$ is RGI. Note finally that the vertex Γ^μ appearing in graph (b_1) of Fig. 2, which is normally bare, has been dressed up, thus converting the original SDE to its Bethe-Salpeter version; evidently, the kernel $\mathcal{K}_{AA\bar\psi\psi}$ must be adjusted accordingly [3,100], in order to avoid overcounting.

Then, suppressing all indices and momenta, the SDE in the bottom panel of Fig. 2 reads

$$\Gamma_R = Z_1 \Gamma^{(0)} + \int_\ell \Gamma_R \mathrm{P} \hat{\mathcal{K}}_{AA\bar\psi\psi}, \quad (3.7)$$

or, using Eq. (3.3), with appropriately assigned momenta,

$$Z_1 \Gamma^{(0)} = L_R \Gamma^{(0)} - \int_\ell L_R \Gamma^{(0)} \mathrm{P} \hat{\mathcal{K}}_{AA\bar\psi\psi}. \quad (3.8)$$

Note the presence of a factor L_R in both terms on the r.h.s. of Eq. (3.8).

Then, returning to Eq. (3.5) and substituting the term $Z_1 \Gamma^{(0)}$ appearing in it by the r.h.s. of Eq. (3.8), one obtains

$$\mathcal{M}(p) = c \int_k \mathrm{Tr}[\Gamma^{(0)} \mathcal{R}_f^2 \Gamma^{(0)} \mathrm{P}] \mathcal{M}(k)$$
$$- c \int_k \int_\ell \mathrm{Tr}[\Gamma^{(0)} \hat{\mathcal{K}}_{AA\bar\psi\psi} \mathcal{R}_f^2 \Gamma^{(0)} \mathrm{PP}] \mathcal{M}(k). \quad (3.9)$$

Then, after neglecting the second ("higher-order") term on the r.h.s. of Eq. (3.9), one recovers precisely Eq. (3.6); thus, as announced, the above analysis boils down to the effective replacement $Z_1 \Gamma_\nu^{(0)} \to L_R(q) \Gamma_\nu^{(0)}$.

C. Further remarks

We point out that the renormalization procedure adopted in [82] is conceptually identical to the one presented above, but is operationally distinct, due to the use of an alternative set of approximations. In particular: (i) The ghost dressing function, $F(q)$, enters into the gap equation through the STI that Γ_ν satisfies; its renormalization is given by $F_R(q) = Z_c^{-1} F(q)$. (ii) In the Landau gauge, $Z_1 = Z_c^{-1}$ to lowest order; the replacement of Z_1 by Z_c^{-1} is therefore carried out at the level of the gap equation. (iii) In the Taylor renormalization scheme [104], the combination $\mathcal{R}_F(q) = g\Delta^{1/2}(q) F(q)$ is RGI. (iv) By virtue of a special exact relation [86,105], we have $Z_c = Z_G$.

Then, the construction presented in Sec. III A gets modified; one considers the product $gZ_c^{-1} \Delta^{1/2}(q)$ and converts it into a cutoff-independent RGI combination through replacing Z_c^{-1} by a function of q^2. Due to property (iv), this may be accomplished in two obvious ways, namely by converting it to either $\mathcal{R}_F(q)$ or to $\mathcal{R}_G(q)$, which amounts to $Z_c^{-1} \to F(q)$ or $Z_c^{-1} \to [1 + G]^{-1}(q)$, respectively.

In conclusion, the effective approaches of implementing multiplicative renormalizability at the level of the quark gap equation may be summarized by the statement that one carries out the substitution $Z_1 \Gamma_\nu^{(0)} \to \mathcal{C}_1(q) \Gamma_\nu^{(0)}$, where, depending on the particular details and approximations

$$\mathcal{C}_1(q) = L_R(q), \qquad \mathcal{C}_1(q) = F_R(q),$$
$$\mathcal{C}_1(q) = [1 + G_R(q)]^{-1}. \quad (3.10)$$

It is important to mention that all three possibilities for $\mathcal{C}_1(q)$ listed in Eq. (3.10) have the exact same ultraviolet behavior, giving rise to the correct one-loop anomalous dimension for $\mathcal{M}(p)$ [82]. Quite interestingly, as may be seen in the right panel of Fig. 2, these three functions are

very similar in the entire range of momenta; as a result, the solutions for $\mathcal{M}(p)$ obtained by inserting any one of them in the gap equation are rather close to each other [82].

D. Effective renormalization of the gluon mass equation

We now return to the main objective of this section, and model the multiplicative renormalization of the gluon mass equation following a method completely analogous to the one outlined above.

To begin with, let us point out that, unlike $\mathcal{M}(p)$, the $m^2(q)$ is *not* RGI. Nonetheless, the quark construction may be followed closely, by simply introducing, for the purposes of this discussion, the dimensionless RGI quantity $\bar{m}^2(q) := m^2(q)/m^2(0)$. Then Eq. (2.8) remains the same, except for the substitutions $m^2(q) \to \bar{m}^2(q)$ and $m^2(k) \to \bar{m}^2(k)$ on its l.h.s and r.h.s, respectively, which are trivially implemented after dividing both sides by the (nonvanishing) $m^2(0)$.

To proceed further, let us consider $\Gamma_3(q_1, q_2, q_3)$ and $\Gamma_4(p_1, p_2, p_3, p_4)$, and simplify their structures, in a way analogous to what was done in Eq. (3.3) for $\Gamma_\nu^R(-p, k, q)$. To that end, consider a single form factor for each vertex, proportional to their corresponding tree-level structures, namely

$$\Gamma_3(q_1, q_2, q_3) \to \mathcal{C}_3(s)\Gamma_3^{(0)}(q_1, q_2, q_3),$$
$$\Gamma_4(p_1, p_2, p_3, p_4) \to \mathcal{C}_4(s)\Gamma_4^{(0)}(p_1, p_2, p_3, p_4), \quad (3.11)$$

where s denotes the so-called "symmetric point," namely the scale associated with the totally symmetric configuration.[6] Specifically, in the case of Γ_3, this special configuration amounts to the choice $q_1^2 = q_2^2 = q_3^2 := s^2$ and $q_i \cdot q_j = -s^2/2$ $(i \neq j)$; similarly, in the case of Γ_4, one has $p_1^2 = p_2^2 = p_3^2 = p_4^2 := s^2$ and $q_i \cdot q_j = -s^2/3$ $(i \neq j)$ (see, e.g., Eq. (2.2) of [106]).

In addition, we introduce the following two RGI combinations [67],

$$\mathcal{R}_3(s) = g\Delta^{3/2}(s)\mathcal{C}_3(s), \qquad \mathcal{R}_4(s) = g^2\Delta^2(s)\mathcal{C}_4(s),$$
$$(3.12)$$

which, due to the particular kinematics chosen, depend only on a single variable s.

Then, the two strings appearing on the r.h.s. of Eq. (2.13) may be reexpressed as

$$Z_3 g_R^2 \Delta_R^2 [1 + G_R(q)]^{-1} = Z_3 \mathcal{C}_{3R}^{-1}\mathcal{R}_G\mathcal{R}_3,$$
$$Z_4 g_R^4 \Delta_R^4 \mathcal{C}_{3R}[1 + G_R(q)]^{-1} = Z_4 \mathcal{C}_{4R}^{-1}\mathcal{R}_G\mathcal{R}_3\mathcal{R}_4. \quad (3.13)$$

Therefore, one may rewrite Eq. (2.8) in the following schematic form (suppressing irrelevant kinematic factors)

---

[6] The symmetric points of the two vertices may be chosen to be different, say s_1 and s_2, instead of the common s, without affecting the central argument.

$$\bar{m}^2(q) \sim \int_k \bar{m}^2(k)\{Z_3\mathcal{C}_{3R}^{-1}\mathcal{R}_G\mathcal{R}_3 + Z_4\mathcal{C}_{4R}^{-1}\mathcal{R}_G\mathcal{R}_3\mathcal{R}_4\},$$
$$(3.14)$$

which is the analogue of Eq. (3.5). Then, following essentially the same reasoning, one implements the substitutions $Z_3 \to \mathcal{C}_{3R}$ and $Z_4 \to \mathcal{C}_{4R}$, or, equivalently, setting $s = k$,

$$\mathcal{K}_R^+(q, k) \to \mathcal{K}_{\text{eff}}^+(q, k) = \mathcal{C}_4(k)[Y(k+q) + Y(k)] - \mathcal{C}_3(k),$$
$$\mathcal{K}_R^-(q, k) \to \mathcal{K}_{\text{eff}}^-(q, k) = \mathcal{C}_4(k)[Y(k+q) - Y(k)].$$
$$(3.15)$$

This final step is depicted in panel (D) of Fig. 1.

E. "Solving" for Z_3 and Z_4 from the vertex SDEs

The construction presented in Sec. III B may be repeated for the case in hand, by considering the SDEs for the vertices Γ_3 and Γ_4, represented in Fig. 3, whose main ingredients are multigluon kernels. In particular, suppressing color and Lorentz indices, we denote by $\mathcal{K}_n$ the amputated kernels with n incoming gluons, and by $\mathcal{K}_n^R$ their renormalized counterparts; the kernels are related to each other by $\mathcal{K}_n^R = Z_A^{\frac{n}{2}}\mathcal{K}_n$. Then, the combinations $\hat{\mathcal{K}}_n = \Delta^{\frac{n}{2}}\mathcal{K}_n$, are clearly RGI.

To illustrate these definitions with an example, consider the "lowest" order dressed contribution to $\mathcal{K}_4$, to be denoted by $\mathcal{K}_4'$, given by

$$\mathcal{K}_4' = g^2\Gamma_3\Delta\Gamma_3 = Z_g^2 Z_3^{-2} Z_A\{g_R^2\Gamma_3^R\Delta^R\Gamma_3^R\} = Z_A^{-2}\mathcal{K}_4'^R.$$
$$(3.16)$$

Then, the $\hat{\mathcal{K}}_4'$ is given by $\hat{\mathcal{K}}_4' = \Delta^2\{g^2\Gamma_3\Delta\Gamma_3\} = \mathcal{R}_3^2$.

Turning to the SDEs, and suppressing strings of projectors P that are totally inert, we have

$$\Gamma_3 = Z_3\Gamma_3^{(0)} + \int_k \Gamma_3\hat{\mathcal{K}}_4 + \int_k \int_\ell \hat{\mathcal{K}}_5\{g\Delta^{1/2}\Gamma_4\} + \cdots,$$
$$\Gamma_4 = Z_4\Gamma_4^{(0)} + \int_k \hat{\mathcal{K}}_5\{g^{-1}\Delta^{-1/2}\Gamma_3\} + \int_k \int_\ell \Gamma_4\hat{\mathcal{K}}_6 + \cdots,$$
$$(3.17)$$

where the ellipses denote the remaining terms of Fig. 3.

Then, from Eq. (3.13), we have that $g\Delta^{1/2}\mathcal{C}_4 = \mathcal{C}_3\mathcal{R}_4\mathcal{R}_3^{-1}$, or, equivalently, $g^{-1}\Delta^{-1/2}\mathcal{C}_3 = \mathcal{C}_4\mathcal{R}_3\mathcal{R}_4^{-1}$. Substituting appropriately, Eq. (3.17) may be expressed as

$$\mathcal{C}_3\Gamma_3^{(0)} = Z_3\Gamma_3^{(0)} + \int_k \mathcal{C}_3\Gamma_3^{(0)}\hat{\mathcal{K}}_4 + \int_k \int_\ell \mathcal{C}_3\Gamma_4^{(0)}\mathcal{R}_4\mathcal{R}_3^{-1}\hat{\mathcal{K}}_5$$
$$+ \cdots,$$

$$\mathcal{C}_4\Gamma_4^{(0)} = Z_4\Gamma_4^{(0)} + \int_k \mathcal{C}_4\Gamma_3^{(0)}\mathcal{R}_3\mathcal{R}_4^{-1}\hat{\mathcal{K}}_5 + \int_k \int_\ell \mathcal{C}_4\Gamma_4^{(0)}\hat{\mathcal{K}}_6$$
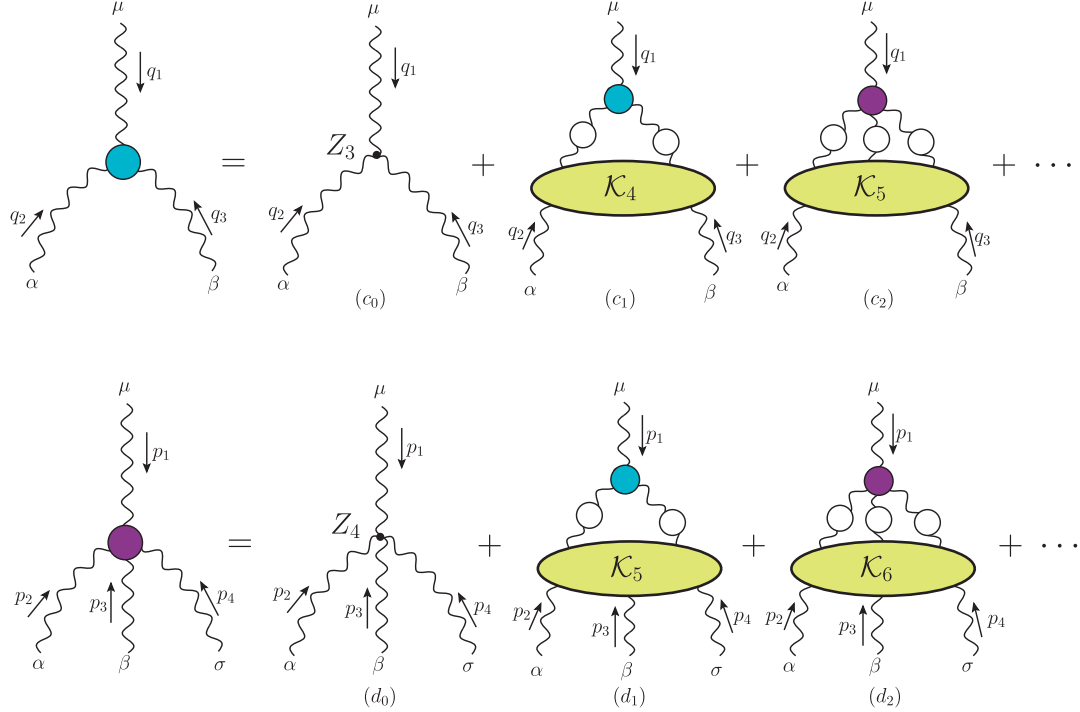$$+ \cdots. \quad (3.18)$$

FIG. 3.   The SDEs for the three-gluon and four-gluon vertices.

Evidently, after this rearrangement, the first equation in Eq. (3.18) involves only $\mathcal{C}_3$, while the second only $\mathcal{C}_4$. Thus, the relations analogous to Eq. (3.8) become

$$Z_3\Gamma_3^{(0)} = \mathcal{C}_3\Gamma_3^{(0)} - \int_k \mathcal{C}_3\left[\Gamma_3^{(0)}\hat{\mathcal{K}}_4 + \int_\ell \Gamma_4^{(0)}\mathcal{R}_4\mathcal{R}_3^{-1}\hat{\mathcal{K}}_5\right]$$
$$- \cdots,$$

$$Z_4\Gamma_4^{(0)} = \mathcal{C}_4\Gamma_4^{(0)} - \int_k \mathcal{C}_4\left[\Gamma_3^{(0)}\mathcal{R}_3\mathcal{R}_4^{-1}\hat{\mathcal{K}}_5 + \int_\ell \Gamma_4^{(0)}\hat{\mathcal{K}}_6\right]$$
$$- \cdots. \tag{3.19}$$

Clearly, and in exact analogy with Eq. (3.8), the omission of the integral contribution of the r.h.s. of both equations leads to the announced heuristic substitution $Z_3\Gamma_3^{(0)} \to \mathcal{C}_3\Gamma_3^{(0)}$ and $Z_4\Gamma_4^{(0)} \to \mathcal{C}_4\Gamma_4^{(0)}$.

IV. THE MAIN INGREDIENTS OF THE NUMERICAL ANALYSIS

In this section, we first cast the mass equation into a form appropriate for its numerical treatment, and subsequently discuss the main characteristics and physical properties of the ingredients entering in it.

In order to solve Eq. (2.8) numerically, we switch to spherical coordinates, introducing the variables $x = q^2$, $y = k^2$, and $z = (k + q)^2 = x + y + 2\sqrt{xy}c_\theta$, where $c_\theta :=$ $\cos\theta$, $s_\theta := \sin\theta$, and

$$\int_k = \frac{1}{(2\pi)^3}\int_{y,\theta}, \qquad \int_{y,\theta} := \int_0^\infty dy\,y \int_0^\pi d\theta s_\theta^2. \tag{4.1}$$

Then, the equation to solve assumes the form

$$m^2(x) = \frac{\alpha_s C_A}{2\pi^2}\frac{1}{x[1 + G(x)]}\int_{y,\theta} z^{-1}\Delta(y)\Delta(z)$$
$$\times [\mathcal{K}_1(x, y, z) + \mathcal{K}_2(x, y, z)]m^2(y), \tag{4.2}$$

where

$$\mathcal{K}_1(x,y,z) = \{\mathcal{C}_4(y)[Y(z)+Y(y)]-\mathcal{C}_3(y)\}(z-y)(3z-xs_\theta^2),$$
$$\mathcal{K}_2(x,y,z) = \mathcal{C}_4(y)[Y(z)-Y(y)][x(z+ys_\theta^2)+2(z-y)^2]. \tag{4.3}$$

As already mentioned in the Introduction, in all previous works Eq. (4.2) has been linearized, by treating the $\Delta(y)$ and $\Delta(z)$ as external inputs, whose form was determined from appropriate fits to the gluon lattice data of [29]. Instead, in the present analysis we maintain the nonlinear nature of Eq. (4.2) intact, by replacing Eq. (2.2) in it, i.e., setting

$$\Delta(t) = [tJ(t) + m^2(t)]^{-1}, \qquad t = y, z. \tag{4.4}$$

We next discuss the main characteristics and physical properties of the various ingredients entering in Eq. (4.2), and in particular of $J(q), \mathcal{C}_3(k), \mathcal{C}_4(k), Y(k)$, and $1 + G(q)$.

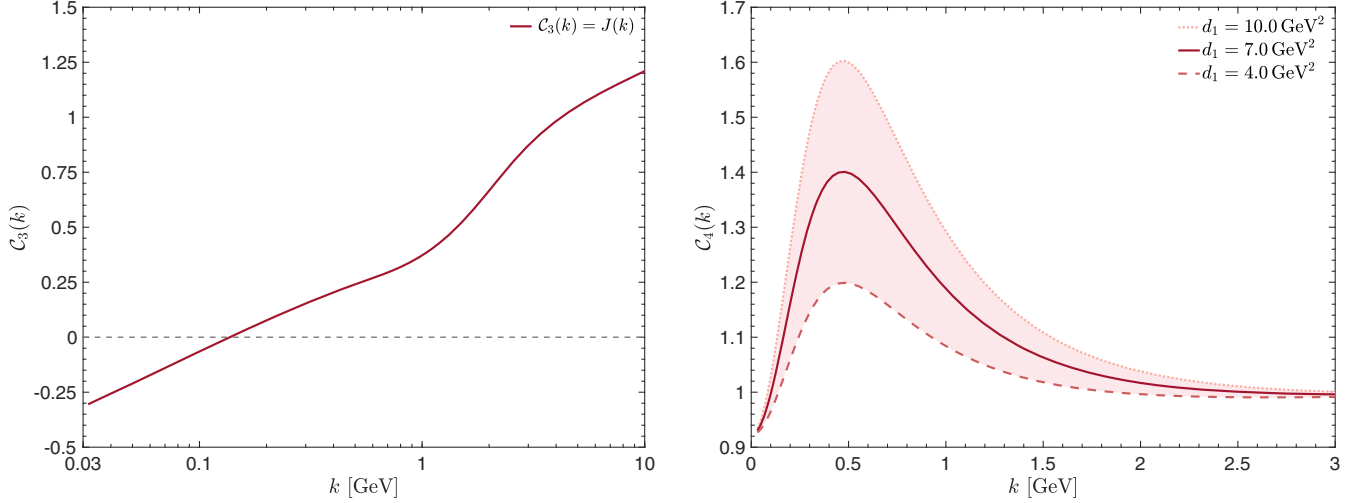FIG. 4.   Left panel: The $\mathcal{C}_3(k)$ employed in the first iteration. Right panel: The $\mathcal{C}_4(k)$ given by Eq. (4.8), with the parameter d_1 varying in the range $(4.0$–$10.0)$ GeV^2.

(i) In order to implement Eq. (4.4), and in the absence of a *bona fide* dynamical equation, a suitable *Ansatz* for $J(q)$ needs to be employed, which will be gradually improved during the iterative procedure (see next section).

In the left panel of Fig. 4 we show the initial seed for $J(q) \to J_0(q)$; it displays the same functional form employed in the recent nonperturbative Ball-Chiu construction of the longitudinal part of the three gluon vertex [69], namely

$$J(q) = 1 + \frac{C_A \lambda_s}{4\pi} \left(1 + \frac{\tau_1}{q^2 + \tau_2} \right)$$
$$\times \left[2 \ln \left(\frac{q^2 + \eta^2(q)}{\mu^2} \right) + \frac{1}{6} \ln \left(\frac{q^2}{\mu^2} \right) \right], \quad (4.5)$$

with

$$\eta^2(q) = \frac{\eta_1}{q^2 + \eta_2}, \quad (4.6)$$

where the fitting parameters for $J_0(q)$ are quoted in Table I. It is important to emphasize that, throughout this work, the renormalization point will be fixed at $\mu = 4.3$ GeV.

TABLE I.   The fitting parameters for $J_i(q)$ whose functional form is given by Eq. (4.5). $J_0(q)$ is the initial *Ansatz* presented in Fig. 4, while $J_1(q)$, $J_2(q)$, and $J_3(q)$ are the solutions shown in the top right panel of Fig. 7.

$J(q)$	λ_s	$\tau_1[\text{GeV}^2]$	$\tau_2[\text{GeV}^2]$	$\eta_1[\text{GeV}^4]$	$\eta_2[\text{GeV}^2]$
$J_0(q)$	0.220	9.870	0.910	17.480	1.180
$J_1(q)$	0.243	2.638	0.265	6.451	0.388
$J_2(q)$	0.220	3.503	0.263	8.261	0.454
$J_3(q)$	0.220	2.8	0.201	6.849	0.363

(ii) According to its definition in Eq. (3.11), $\mathcal{C}_3(s)$ is the cofactor of the tree-level structure of $\Gamma_3(q_1, q_2, q_3)$ when all form-factors are evaluated at the symmetric point. In particular, in the Ball-Chiu basis (see Eq. (4.10) and Eq. (3.4) of [69]), we have that, at the symmetric point, $X_1(s) = X_4(s) = X_7(s) :=\mathcal{C}_3(s)$. In general, the $X_i(q, r, p)$ may be expressed in terms of $J(q)$, the ghost dressing function $F(q)$, and three of the five form factors of the so-called ghost-gluon kernel [107]. However, the corresponding nonperturbative evaluation reveals that the "Abelian approximation," obtained by turning off the ghost sector, is numerically rather close to the full answer (see, e.g., Fig. 7 in [69]). Therefore, we will simplify the complexity of our analysis by using the corresponding "Abelian" result (see Eq. (3.13) of [69]), e.g.,

$$\mathcal{C}_3(k) = J(k), \quad (4.7)$$

which is represented in the left panel of Fig. 4. Evidently, since the form of $J(k)$ will vary from one iteration to the next, by virtue of Eq. (4.7) so will $\mathcal{C}_3(k)$.

(iii) Unfortunately, the available functional studies [17,50, 108,109] furnish rather limited information on the nonperturbative properties of the four-gluon vertex, and no lattice simulations have been carried out to date.[7] Therefore, our *Ansatz* for $\mathcal{C}_4(k)$ will be designed to simply capture certain general trends, observed in all aforementioned studies. In particular, for a variety of special kinematic configurations, described by a single momentum scale, the form

---

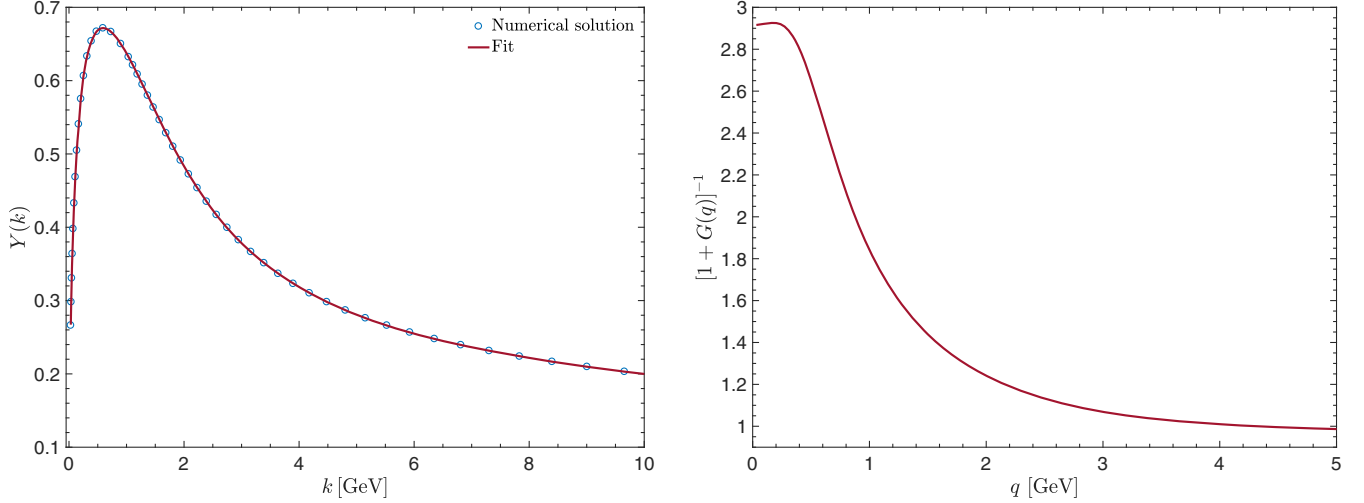[7]See also [106,110] for a variety of relevant properties of the four-gluon vertex.

FIG. 5. Left panel: The numerical solution for $Y(k)$ obtained from Eq. (4.11) (circles), and the corresponding fit given by Eq. (4.13) (continuous). Right panel: The inverse of the auxiliary function, $1 + G(q)$, whose fit is given by Eq. (4.14).

factor accompanying either the $\Gamma_4^{(0)}$ or its *transversely projected counterpart* displays a typical peak, located in the region of a few hundred MeV. Motivated by the above observations, the overall qualitative behavior of $\mathcal{C}_4(k)$ will be modeled by

$$\mathcal{C}_4(k) = 1 + \frac{\lambda}{4\pi}\left[1 - \frac{d_1 k^2}{(k^2 + d_2)^2}\right]\ln\left(\frac{k^2 + 4m_0^2}{\mu^2}\right),$$

(4.8)

where $\lambda = 0.28$, $d_2 = 0.26\,\text{GeV}^2$, and $m_0^2 = 0.14\,\text{GeV}^2$; the corresponding curves are shown on the right panel of Fig. 4. Notice that the red shaded area is created varying the value of d_1 in the range of $(4.0–10.0)\,\text{GeV}^2$, while all other parameters in Eq. (4.8) are kept fixed.

As we will see in the end of Sec. V, these variations of $\mathcal{C}_4(k)$ have no appreciable impact on our solutions, and may be compensated by appropriately re-adjusting the value of α_s. The aspect that seems to be decisive is the moderate enhancement that $\mathcal{C}_4(k)$ displays with respect to its tree-level value (unity) in a region of momenta known to be important for mass generation.

(iv) The determination of $Y(k)$ proceeds by evaluating numerically its defining expression [66]

$$Y(k) = -\frac{1}{4}g^2 C_A \frac{k^\rho}{k^2}\int_\ell \Delta_{\mu\rho}(\ell)\Delta_{\alpha\nu}(\ell + k)\Gamma_3^{\alpha\mu\nu}$$
$$\times (k, \ell, -k - \ell).$$

(4.9)

To that end, we set $\Gamma_3^{\alpha\mu\nu} = \Gamma_{3\mathbf{L}}^{\alpha\mu\nu} + \Gamma_{3\mathbf{T}}^{\alpha\mu\nu}$, where $\Gamma_{3\mathbf{L}}^{\alpha\mu\nu}$ saturates the relevant STIs, while the $\Gamma_\mathbf{T}^{\alpha\mu\nu}$ vanishes when contracted by q_α, r_μ, or p_ν. Keeping only the former term, we have that

$$\Gamma_{3\mathbf{L}}^{\alpha\mu\nu}(q, r, p) = \sum_{i=1}^{10} X_i(q, r, p)\ell_i^{\alpha\mu\nu},$$

(4.10)

where the basis tensors $\ell_i^{\alpha\mu\nu}$ are given in Eq. (3.4) of [69]. After carrying out the various momentum contractions, and passing to spherical coordinates, one arrives at

$$Y(y) = \frac{\alpha_s C_A}{8\pi^2}\int_{t,\omega} s_\omega^2 \Delta(t)\Delta(u)\mathcal{K}_Y(t, y, \omega),$$

(4.11)

where $y = k^2$, $t = \ell^2$, $u = (k + \ell)^2 = y + t + 2\sqrt{yt}c_\omega$,

$$\mathcal{K}_Y(t, y, \omega) = -tX_6 + 6X_7 - (u + y - t)\left[3X_9 + \frac{t}{u}X_3\right]$$
$$+ \frac{(u + t - y)}{2u}[X_4 - 2X_1],$$

(4.12)

and $X_i = X_i(y, t, \omega)$. Note that the additional $\sin^2\omega$ in the angular integral stems from the presence of the common factor $\frac{k^2\ell^2 - (k\cdot\ell)^2}{k^2\ell^2} = s_\omega^2$.

To further evaluate $Y(y)$ through Eq. (4.11) and (4.12), we employ the results for the form factors X_i obtained in [69].[8] The curve obtained is shown in the left panel of Fig. 5; it can be fitted by

$$Y(k) = 3\pi\alpha_s C_A\left\{\left[A\ln\left(\frac{k^2 + \eta^2(k)}{\mu^2}\right) + B\ln\left(\frac{k^2}{\mu^2}\right)\right]\right.$$
$$\left. \times\left[1 + \frac{Ck}{1 + (k^2/\nu^2)^\gamma}\right] + D\right\},$$

(4.13)

---

[8]In earlier works, $Y(k)$ was determined either by setting $\Gamma_{\mu\alpha\beta}(q, r, p) = \Gamma_{\mu\alpha\beta}^{(0)}(q, r, p)$ [66,67], or by using the first relation in Eq. (3.11), where the functional form of $\mathcal{C}_3(s)$, denoted by $f(s)$ in [111], is given by Eq. (5.5) of that article.

where $\eta^2(k)$ is given by Eq. (4.6). The fitting parameters are $A = -0.015$, $B = 0.0095$, $C = 2.158$ GeV, $D = 0.039$, $\nu^2 = 2.422$ GeV^2, $\gamma = 1.074$, $\eta_1 = 0.0103$ GeV^4, and $\eta_2 = 0.184$ GeV^2. As we will see in the next section, the concrete value of α_s will be tuned, for each set of ingredients, at the level of the dynamical equation; the curve shown in the left panel of Fig. 5 is obtained by using $\alpha_s = 0.27$.

(v) The final ingredient is the auxiliary function $1 + G(q)$, introduced in Eq. (2.4), whose inverse is shown in the right panel of Fig. 5. For this function we employ the following fit, which is valid for the entire range of Euclidean momenta [82], namely

$$1 + G(q) = 1 + \frac{9 C_A}{48\pi} [\alpha_g + A_1 \exp(-\rho_1 q^2/\mu^2)]$$
$$\times \ln\left(\frac{q^2 + \rho_2 \eta^2(q)}{\mu^2}\right), \quad (4.14)$$

where $\eta^2(q)$ is also given by Eq. (4.6), but now with $\eta_1 = 0.30$ GeV^4, $\eta_2 = 0.33$ GeV^2. The remaining adjustable parameters are $\alpha_g = 0.21$, $A_1 = 0.77$ GeV^2, $\rho_1 = 0.78$, and $\rho_2 = 0.50$.

V. SOLUTIONS OF THE NONLINEAR MASS EQUATION

Having defined all necessary inputs, in this section we discuss in detail the solutions obtained from the numerical treatment of the gluon mass equation.

A. General qualitative observations

Before embarking on the full analysis, we address certain qualitative issues related with this particular equation.

We start by observing that, as $x \to 0$, Eq. (4.2) reduces itself to the following nontrivial constraint

$$m^2(0) = -\frac{3 C_A \alpha_s}{8\pi} [1 + G(0)]^{-1} \int_0^\infty dy\, m^2(y) \mathcal{K}_0(y), \quad (5.1)$$

where

$$\mathcal{K}_0(y) = \mathcal{C}_3(y)[y^2 \Delta^2(y)]' - 2\mathcal{C}_4(y)[y^2 \Delta^2(y) Y(y)]'. \quad (5.2)$$

Note that, when $\mathcal{C}_3(y) = \mathcal{C}_4(y) = 1$, Eq. (5.1) collapses to Eq. (8.11) of [66].[9] Equation (5.1) is especially useful, because it captures in a relatively simple expression some of the crucial features displayed by the full equation.

We start by highlighting the impact that $\mathcal{C}_3(k)$ and $\mathcal{C}_4(k)$ have on the structure of the kernel (5.2). Specifically, the net effect of both functions is to broaden considerably the

---

[9]We emphasize that, for convenience, the definition of $Y(k)$ in Eq. (4.3) *absorbs* a factor $C = 3\pi\alpha_s C_A$, which in [66] multiplies explicitly the Y terms.

negative support of the kernel with respect to the case $\mathcal{C}_3(y) = \mathcal{C}_4(y) = 1$ [see left panel of Fig. 6]; consequently, the equation may accommodate comfortably a positive-definite $m^2(y)$.

Furthermore, it is important to emphasize from the outset that, contrary to what happens in the linearized case [66,67], where solutions exist only for a unique value of α_s, the nonlinearized equation yields solutions for a continuous (and rather extended) interval of values for α_s. The simplest way to establish this is to vary α_s keeping the form of $J(q)$ fixed, and observe that one obtains a continuous family of $m^2(q)$ [see right panel of Fig. 6]. Of course, the $m^2(q)$ so obtained, when put together with the $J(q)$ in the combination of Eq. (2.2), give rise to gluon propagators that, in general, have little or nothing to do with the lattice results for $\Delta(q)$. As we will see below, in order to approach the lattice data, the values of α_s must be chosen from a rather narrow interval.

B. Full numerical analysis: Results and discussion

The numerical procedure: The numerical solution for $m^2(q)$ is obtained through an iterative procedure consisting of the following main steps:

(s_0): An excellent numerical fit to the gluon lattice data of [29] is employed, to be denoted by $\Delta_L(q)$; its functional form is given in Eq. (4.1) of [81]. In particular, we fix the fitting parameters such that $\Delta_L^{-1}(0) = 0.14$ GeV^2.

(s_1): We begin the iteration by introducing two initial seeds, one for $m^2(q)$ and another one for $J(q)$. For $m^2(q)$ we use a random function, while for $J(q)$ the *Ansatz* of Eq. (4.5), i.e., we set $J(q) \to J_0(q)$; the corresponding fitting parameters are quoted in Table I.

(s_2): With these starting ingredients, we solve Eq. (4.2) iteratively, adjusting the value of α_s such that $m^2(0) = \Delta_L^{-1}(0)$. The solution is accepted when the relative difference between two successive results for $m^2(q)$ is below 10^{-5}; we denote this solution by $m_{s_2}^2(q)$.

(s_3): The $m_{s_2}^2(q)$ is combined with the $J_0(q)$ as dictated by Eq. (2.2), in order to obtain our approximation for $\Delta(q)$, which is then compared with $\Delta_L(q)$.

(s_4): In order to improve the result of (s_3), we determine a new $J(q)$, which will be used to obtain from Eq. (4.2) a new solution for $m^2(q)$. This new $J(q)$ is obtained from Eq. (2.2), i.e., $J(q) = [\Delta_L^{-1}(q) - m_{s_2}^2(q)]/q^2$. The resulting $J(q)$ is fed into Eq. (4.2), and the step (s_2) repeated.

(s_5): The steps (s_2)–(s_4) are repeated, saving those combinations of $m^2(q)$ and $J(q)$ which best reproduce $\Delta_L(q)$.

In Fig. 7 we present the outcome of the procedure described above, for three different cases of $J(q)$. In particular, we show the best results obtained for each case, which occur when $\alpha_s = 0.272$ (blue dashed dotted curves), $\alpha_s = 0.278$ (red dashed), and $\alpha_s = 0.289$ (yellow dotted).
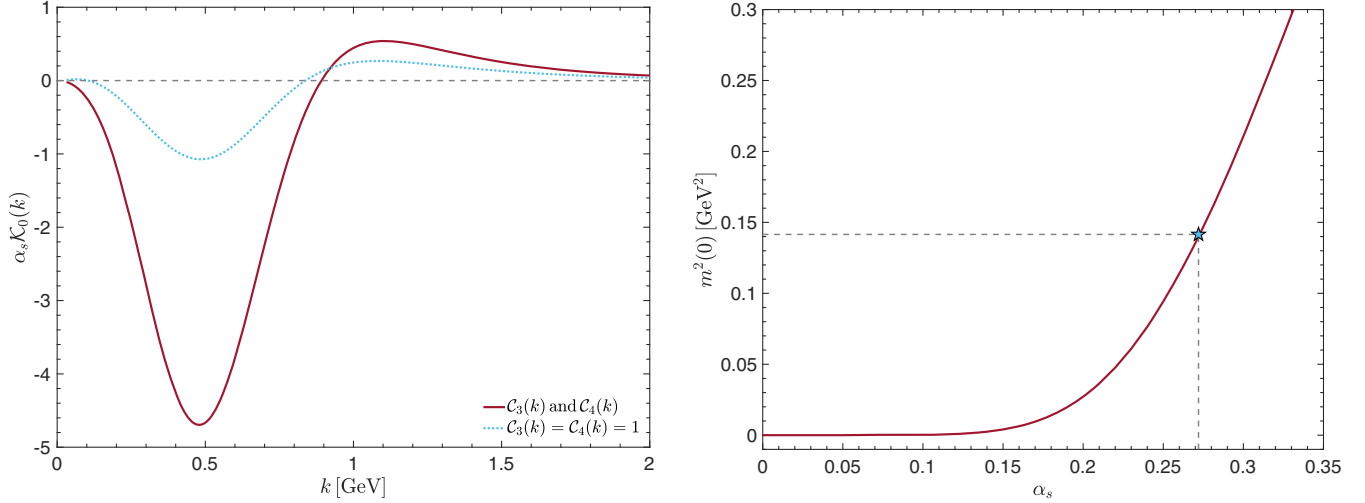
FIG. 6. Left panel: The kernel $\alpha_s \mathcal{K}_0(k)$ defined by Eq. (5.2) for (i) $\mathcal{C}_3(y)$ and $\mathcal{C}_4(y)$ given by Eqs. (4.7) and (4.8), respectively (red continuous), and (ii) for $\mathcal{C}_3(y) = \mathcal{C}_4(y) = 1$ (blue dotted). For both cases we have used $\alpha_s = 0.27$. Right panel: The values of $m^2(0)$, obtained from solving Eq. (4.2) for a *fixed* $J(q)$, as function of α_s. The blue star denotes the α_s that reproduces the lattice value $m^2(0) = 0.14$.

As mentioned at step (s_2) above, these values of α_s are essentially determined from the requirement that $\Delta_L(0) = m^{-2}(0)$. Evidently, this condition is rather restrictive, forcing α_s to take values within a rather small interval, i.e., $\alpha_s \in [0.272, 0.289]$, with the renormalization point fixed at $\mu = 4.3$ GeV. Quite interestingly, this range is completely compatible with the analysis of [104], and is particularly close to $\alpha_s = 0.32$, which is the estimated value of the coupling used in the lattice simulations of [77,79].

It becomes clear from the top panels of Fig. 7, that small variations in the $J(q)$ can be compensated by minor adjustments in the value of α_s, producing basically the same solution for $m^2(q)$.

In what follows, we will comment on the main characteristics of each plot shown in Fig. 7 and their subsequent applications.

(i) We start with the *dynamical gluon mass*, $m^2(q)$, shown in the top left panel. As one can clearly see, $m^2(q)$ is positive-definite and monotonically decreasing in the entire range of momenta. In addition, it may be accurately fitted with the characteristic power-law running given by

$$m^2(q) = \frac{m_0^4}{\mu_1^2 + q^2 \ln\left[(q^2 + \mu_2^2)/\lambda^2\right]}, \quad (5.3)$$

where the fitting parameters are fixed at $m_0^4 = 0.107$ GeV^4, $\mu_1^2 = 0.756$ GeV^2, $\mu_2^2 = 0.266$ GeV^2, and $\lambda^2 = 0.123$ GeV^2.

We emphasize that this particular fit is superior to previous ones put forth in the related literature [14,69], (e.g., $m^2(q^2) = m_0^2/[1 + (q^2/\lambda^2)^{1+\gamma}], \gamma > 0$), because it captures faithfully not only $m^2(q)$, but

also its first derivative with respect to q^2, to be denoted by $\dot{m}^2(q)$. In particular, as we can verify in the left panel of Fig. 8, the result of the differentiation of the fit in Eq. (5.3) is practically identical to the numerical differentiation of the "raw" data for $m^2(q)$. In fact, one may easily establish that the aforementioned suboptimal fit yields a derivative that vanishes at the origin, a feature which is certainly not shared by the actual numerical solution. The importance of reproducing correctly this derivative is related to the fact that the quantity $-\dot{m}^2(q)$ is *exactly* equal to the Bethe-Salpeter amplitude that controls the formation of the massless excitation that triggers the Schwinger mechanism, and the subsequent generation of a gluon mass [87,111] [see also the related discussion in Sec. VI].

In addition, as stated in Sec. III A, in the right panel of Fig. 8 we show that $m^2(q)$ is independent of the ultraviolet cutoff Λ^2, introduced for the numerical evaluation of the "radial" part of Eq. (4.1). Specifically, we vary Λ^2 in the range of $(10^3 - 10^7)$ GeV^2, and we clearly observe that all curves lie on top of each other.

(ii) The *kinetic term* $J(q)$ is shown in the top right panel of Fig. 7, for three values of α_s. Evidently, the three curves $J_i(q)$ ($i = 1, 2, 3$) are mild variations of the initial *Ansatz* $J_0(q)$ shown in Fig. 4; their differences are related with the location of the zero crossing, which is shifted toward lower momenta with respect to $J_0(q)$, and the "bending" displayed in the intermediate region. In particular, the zero crossings are located at $q = 78$ MeV (blue dashed dotted), $q = 96$ MeV (red dashed), and $q = 90$ MeV (yellow
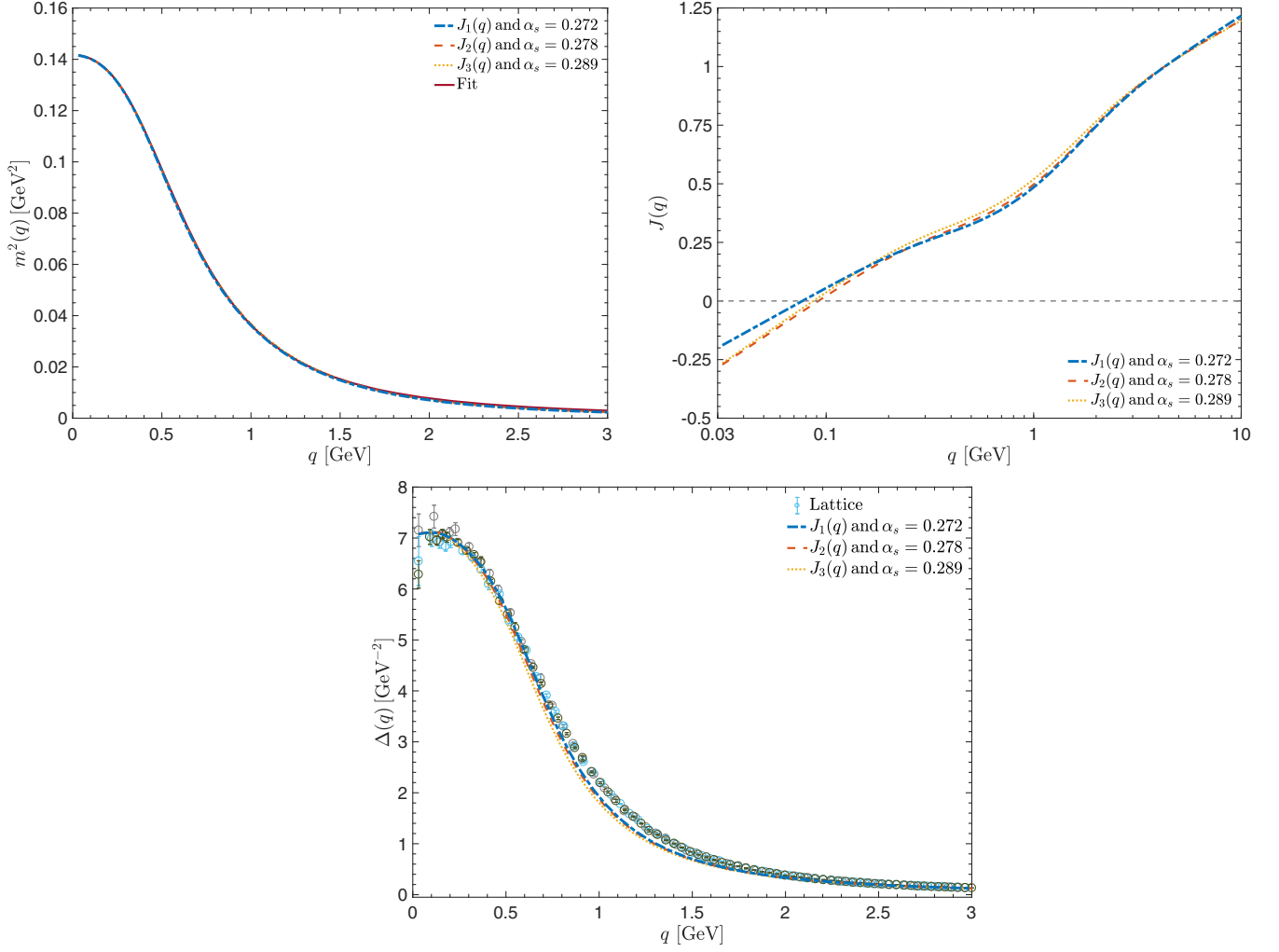
FIG. 7. Top left panel: The numerical results for the dynamical gluon mass $m^2(q)$, for $\alpha_s = 0.272$ (blue dashed dotted), $\alpha_s = 0.278$ (red dashed), and $\alpha_s = 0.289$ (yellow dotted). Top right panel: The corresponding kinetic term $J(q)$. Bottom panel: The resulting gluon propagator $\Delta(q)$ obtained from Eq. (2.2). The lattice data is from [29]. In all plots, we employ the same color code.
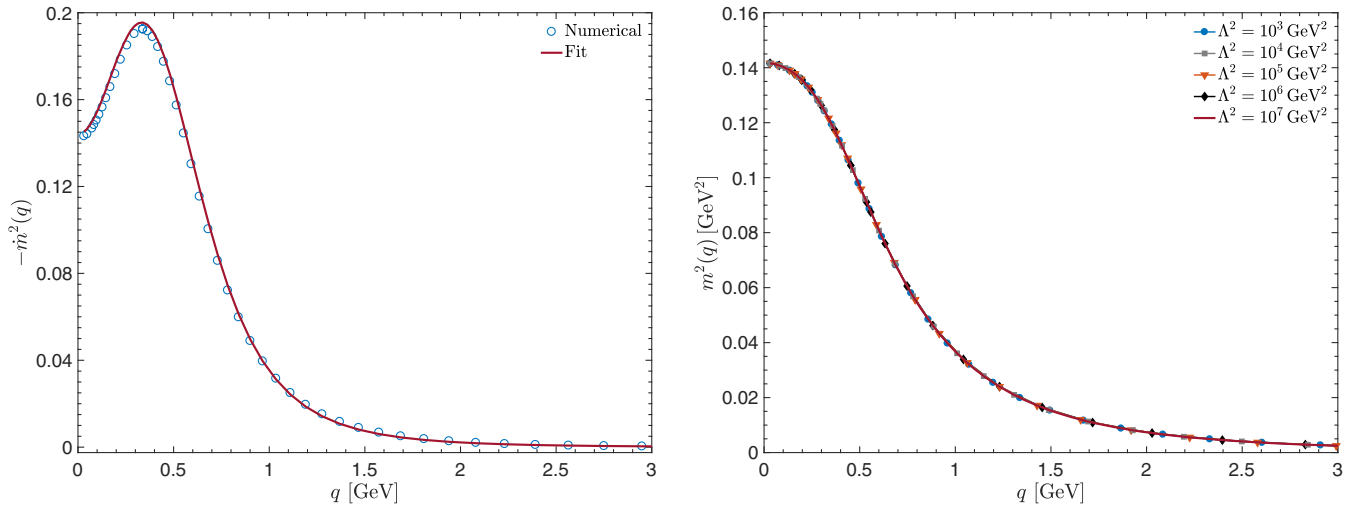

FIG. 8. Left panel: Comparison of the quantity $-\dot{m}^2(q)$ obtained from differentiating (i) the numerical data (blue circles), and (ii) the fit given in Eq. (5.3) (red continuous curve). Right panel: The cutoff-independence of the numerical solution for $m^2(q)$.
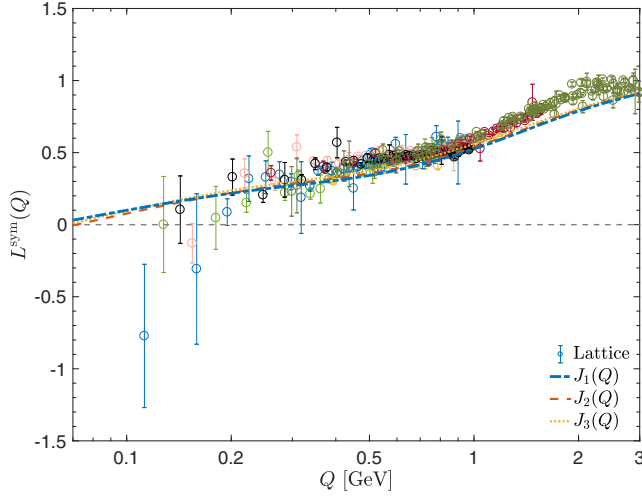
FIG. 9.   Comparison between the lattice data of [77] and the $L^{\text{sym}}(Q)$ obtained using as input the $J_i(q)$ of Fig. 7.

dotted). We note that the $J_i(q)$ may also be fitted by the same functional form as the initial *Ansatz* $J_0(q)$, namely Eq. (4.5); the corresponding fitting parameters for the three cases are quoted in Table I.

An interesting check of the overall quality of the $J_i(q)$ shown above may be obtained by means of the connections established in [69]. As was explained there, the nonperturbative generalization of the Ball-Chiu construction [112] allows one to express the "longitudinal" form factors of the three-gluon vertex $\Gamma_3^{\mu\alpha\beta}(q, r, p)$ in terms of the kinetic term $J(q)$ and three of the components of the so-called ghost-gluon kernel [107]. The form factors so obtained may be then used to estimate some of the quantities measured in lattice simulations of the three-gluon vertex [77]. One typical such quantity, denoted by $L^{\text{sym}}(Q)$, involves a special combination of vertex form factors evaluated at the symmetric point ($q^2 = r^2 = p^2 = Q^2$); for its exact definition, see [69,77].

In Fig. 9, we compare the lattice data of [77] with the results for $L^{\text{sym}}(Q)$ obtained by substituting the $J_i(q)$ of Fig. 7 into the Ball-Chiu solution given in Eq. (3.11) of [69]; evidently, the general shape of the lattice data is reproduced rather accurately. Note that, since the iteration procedure shifts the zero-crossing of each $J_i(q)$ toward the infrared, the corresponding zero-crossing of $L^{\text{sym}}(Q)$ display the same tendency, being at 59 MeV, 76 MeV, and 70 MeV, respectively. This result is to be contrasted with the left panel of Fig. 16 in [69], where the predicted zero-crossing of $L^{\text{sym}}(Q)$ occurs at higher momenta (109–155) MeV.

(iii) The comparison of our results for the *gluon propagator*, $\Delta(q)$, with the lattice data of [29] is shown in the bottom panel of Fig. 7; one can see that the pairs, $J_i(q)$ and $m^2(q)$, reproduce rather well the lattice

data in the entire range of momenta. Notice that the largest discrepancy between our calculated $\Delta(q)$ and the lattice data occurs in the region of momenta between (0.8–2.5) GeV, where the relative error ranges from [0.1–0.15] for $J_1(q)$ (blue dashed dotted curve), [0.1–0.16] for $J_2(q)$ (red dashed), and [0.1–0.2] for $J_3(q)$ (yellow dotted curve). For lower momenta, the relative errors drop considerably, becoming of the order of 10^{-2}. Clearly, the intermediate region is more sensitive to the truncations and approximations implemented; nonetheless, it is quite notable that our solution for $\Delta(q)$ reproduces very well the entire momenta range, by appropriately tuning the value of α_s.

(iv) We next analyze the stability of our solutions under variations in the shape of $\mathcal{C}_4(k)$. To that end, we solve Eq. (4.2) using *seven* curves for $\mathcal{C}_4(k)$, which are all located in the shaded band shown in the right panel of Fig. 4. The curves are obtained by varying in Eq. (4.8) the parameter d_1, which controls the height of the peak. In the left panel of Fig. 10 we show the relation between the maximum value of $\mathcal{C}_4(k)$ and α_s, as d_1 is varied within the range $(4.0–10.0)$ GeV^2. It is clear that, as one reduces the peak range of $\mathcal{C}_4(k)$, the value of α_s increases. In addition, observe that as the peak of $\mathcal{C}_4(k)$ is approaching the unity (tree-level value), α_s tends to values higher than 0.3. Therefore, from this analysis, it is clear that changes in the peak height (area) of $\mathcal{C}_4(k)$ can be counterbalanced with adjustments in the value of α_s, producing essentially the same solution for $m^2(q)$.

There is a simple way to verify that the same $m^2(q)$ is indeed obtained, by comparing the overall shape of the integrand $\alpha_s \mathcal{K}_0(k)$, defined in Eq. (5.2), for different $\mathcal{C}_4(k)$. In the right panel of Fig. 10 we plot $\alpha_s \mathcal{K}_0(k)$, for the variations of $\mathcal{C}_4(k)$ shown in the right panel of Fig. 4. Specifically, the curves are obtained by fixing the values of the pair $(d_1; \alpha_s)$ at (i) $(4.0 \text{GeV}^2; 0.296)$ (dashed), (ii) $(7.0 \text{ GeV}^2; 0.272)$ (continuous), and (iii) $(10.0 \text{ GeV}^2; 0.253)$ (dotted). It is important to emphasize that the α_s used for each curve is different, being determined from the procedure of solving Eq. (4.2) for each $\mathcal{C}_4(k)$. As can be clearly seen in Fig. 10, all curves merge into one another; plainly, the sets $(\alpha_s, \mathcal{C}_4)$ conspire to eventually create the exact same result for $\alpha_s \mathcal{K}_0(k)$. Evidently, since this latter quantity remains practically unchanged, the constraint of Eq. (5.1) produces always the same value, $m^2(0) = 0.14$.

C. Tuning the value of α_s

At first sight, Eq. (4.2) appears to be particularly sensitive to changes in α_s. As can be observed in the bottom panel of Fig. 7, this sensitivity forces us to tune α_s with three-decimal
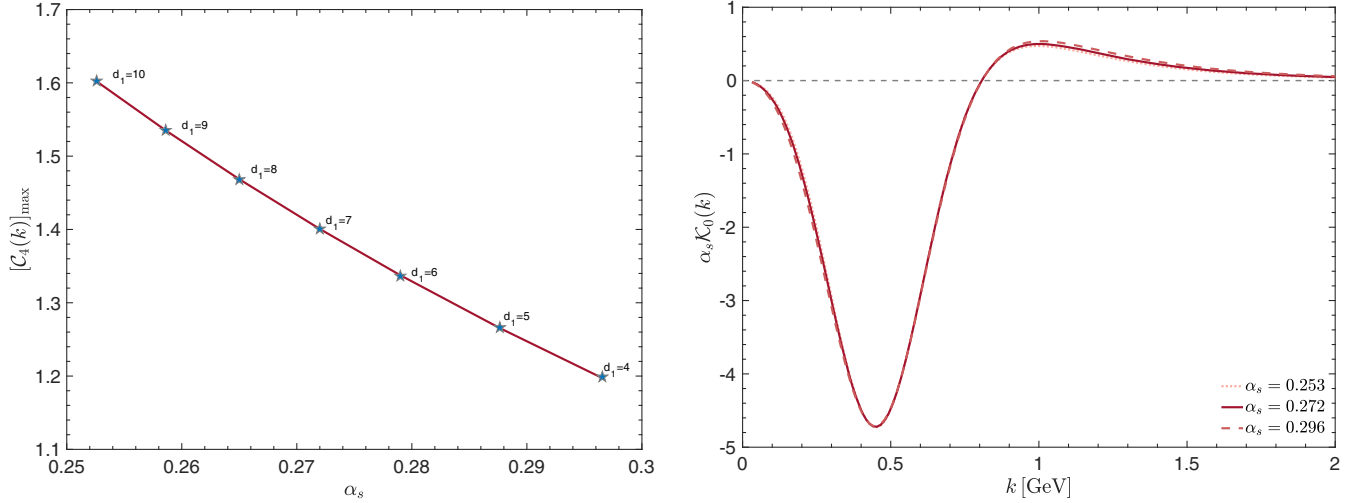
FIG. 10. Left panel: The values of α_s as a function of the peak height of the $\mathcal{C}_4(k)$ shown in Fig. 4. The values of d_1 are in units of GeV^2. Right panel: The response of $\alpha_s \mathcal{K}_0(k)$, defined in Eq. (5.2), to the combined variations of $\mathcal{C}_4(k)$ and α_s.

accuracy in order to reproduce the lattice value $\Delta(0)$ [29]; we remind the reader that the renormalization (subtraction) point is chosen at $\mu = 4.3$ GeV.

To analyze in some depth the response of Eq. (4.2) to variations of α_s, we next determine the amount by which one may vary it and still obtain a $\Delta(0)$ lying within the error bars of the lattice data [29].

To that end, we select our result obtained with $J_1(q)$ (the blue dashed dotted curves in Fig. 7), and vary α_s around its central value $\alpha_s = 0.272$. The result of this procedure is shown in the left panel of Fig. 11, where it can be clearly seen that it is possible to cover the spread of the lattice data (in the infrared region) by varying α_s only by $\pm 1\%$. The corresponding range of solutions for $m^2(q)$ is represented in the right panel of the same figure.

It turns out that the precision in the value of α_s found above may be understood by means of a relatively simple argument.

In particular, from Eq. (2.16),

$$\hat{d}(q) := \mathcal{R}_G^2/4\pi = \frac{\alpha_s \Delta(q)}{[1 + G(q)]^2}, \qquad (5.4)$$

and therefore

$$\hat{d}^{-1}(0) = \alpha_s^{-1}[1 + G(0)]^2 \Delta^{-1}(0). \qquad (5.5)$$

Given that $\hat{d}^{-1}(0)$ is RGI and has dimensions of mass-squared, to lowest order it may be written in the form

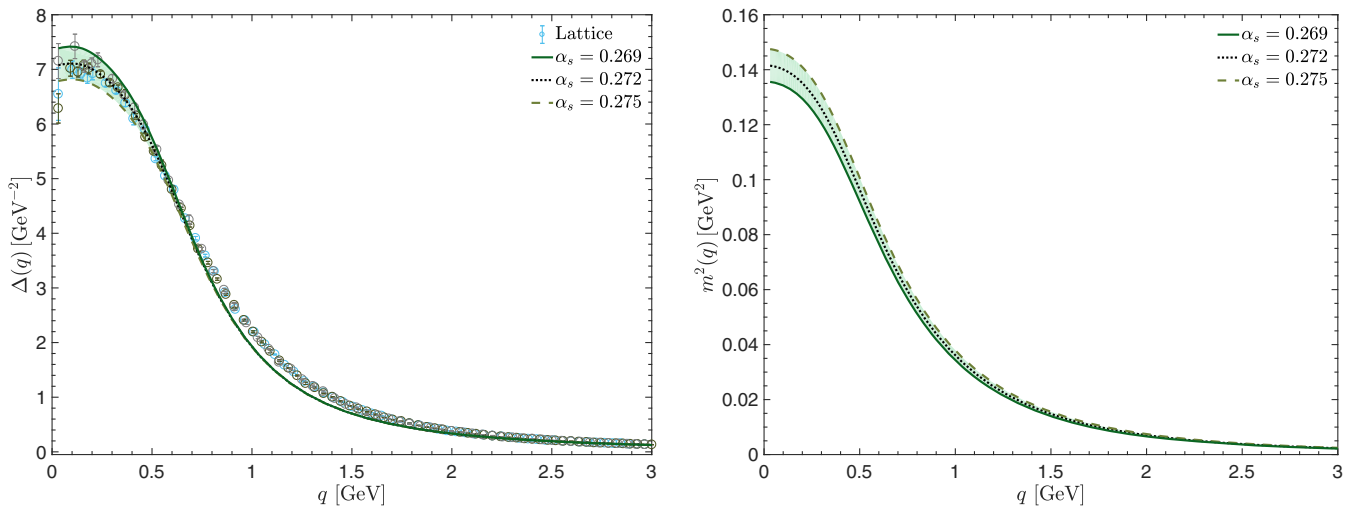$$\hat{d}^{-1}(0) = c\mu^2 \exp\left(-1/\tilde{b}\alpha_s\right), \qquad (5.6)$$

FIG. 11. Left panel: The spreads in the solutions for $\Delta(q)$ when α_s varies $\pm 1\%$. The lattice data are from [29]. Right panel: The corresponding $m^2(q)$.

with $\tilde{b} := 4\pi b$, where b is the first coefficient of the Yang-Mills β function, $\mu(dg/d\mu) = -bg^3$ (for SU(3), $b = 11/16\pi^2$, $\tilde{b} = 11/4\pi$), and c is a (positive) numerical constant.

Then, substituting the r.h.s. of (5.5) into the l.h.s. of Eq. (5.6) yields

$$\Delta^{-1}(0) = c\mu^2[1 + G(0)]^{-2}\alpha_s \exp\left(-1/\tilde{b}\alpha_s\right). \quad (5.7)$$

Next, denote by δf the variation in the value of a quantity f. If the only source for the variation $\delta\Delta^{-1}(0)$ is the corresponding variation $\delta\alpha_s$ in the value of α_s, then from Eq. (5.7) we obtain

$$\frac{\delta\alpha_s}{\alpha_s} = -\sigma\frac{\delta\Delta(0)}{\Delta(0)}, \quad (5.8)$$

where we used that $\delta\Delta^{-1}(0)/\Delta^{-1}(0) = -\delta\Delta(0)/\Delta(0)$, and introduced

$$\sigma := \frac{\tilde{b}\alpha_s}{1 + \tilde{b}\alpha_s}. \quad (5.9)$$

Note that the minus sign accounts precisely for the tendency shown in the left panel of Fig. 11; namely, an increase (decrease) in the value of α_s results in a corresponding decrease (increase) to the value of $\Delta(0)$.

Taking absolute values, and employing the short-hand notation $E_f := \delta f/f$, we have that

$$E_{\alpha_s}/E_{\Delta(0)} = \sigma. \quad (5.10)$$

From the numerical analysis (see also left panel of Fig. 11), we have that $E_{\alpha_s} \approx 10^{-2}$, while $E_{\Delta(0)} \approx 4.3 \times 10^{-2}$, so that $E_{\alpha_s}/E_{\Delta(0)} \approx 0.24$. On the other hand, when we plug into Eq. (5.9) the "central" value $\alpha_s \approx 0.272$ (at $\mu = 4.3$ GeV) we find that $\sigma \approx 0.19$, concluding that Eq. (5.10) is satisfied reasonably well. This simple ballpark estimate seems to indicate that the required tuning in the value of α_s is compatible with what one would expect on general grounds, and is, in that sense, fairly natural.

VI. DISCUSSION AND CONCLUSIONS

In this work we have demonstrated how the nonlinear treatment of the gluon gap equation, in conjunction with an effective implementation of multiplicative renormalization, fixes the value of the emergent gluonic scale, and gives rise to positive-definite and monotonically decreasing running gluon masses. In particular, the analysis presented relies on the following pivotal points:

(i) The nonlinearization of the equation proceeds by implementing Eq. (2.2) for the gluon propagators appearing in it; this substitution, in turn, introduces the unknown function $m^2(q)$ in the corresponding

denominators, thus eliminating the freedom of rescaling the solutions.

(ii) For the kinetic term $J(q)$, entering into the mass equation after the use of Eq. (2.2), we employ physically motivated *Ansätze* which capture its salient features, and are further refined during the iterative numerical procedure.

(iii) An effective approach to multiplicative renormalization, inspired from analogous studies in the quark sector of the theory, has been implemented, which introduces into the mass equation two additional form-factors, one for the three-gluon and one for the four-gluon vertex.

(iv) Due to the inclusion of these form factors, the "competition" between the one- and two-loop terms comprising the mass equation (carrying a relative minus sign) is tilted slightly in favor of the latter. In particular, the infrared suppression of the three-gluon vertex reduces the size of the one-loop term, while the enhancement of the four-gluon form factor boosts up the two-loop contribution, such that, eventually, solutions with the desired properties are obtained.

(v) In various demonstrations throughout this article, and especially in Sec. III, we have relied extensively on special RGI combinations, whose use renders the relevant constructions considerably more transparent.

It is interesting to comment on the relevance of the quantity $-\dot{m}^2(q)$, plotted in the left panel of Fig. 8. As has been explained in a series of works (see e.g., [87,111]), on theoretical grounds this quantity is exactly equal to the Bethe-Salpeter amplitude that controls the formation of the massless excitations that trigger the Schwinger mechanism, and the subsequent generation of a gluon mass. Evidently, the levels of accuracy achieved in fulfilling this equality provide a highly nontrivial check of the entire mechanism, in general, and of the veracity of the approximations employed, in particular. A direct comparison between Fig. 8 of the present work and Fig. 5 of [111] reveals that while the qualitative behavior is similar, the corresponding maxima are relatively further apart [340 MeV and 1 GeV, respectively]. Note, however, that all existing analyses of this particular Bethe-Salpeter equation are also linear, in the sense that, as in the case of the mass equation, the gluon propagators entering in it were treated as external quantities. It turns out that a nonlinear approach to this problem amounts to solving a rather complicated integro-differential equation, whose numerical treatment is already underway.

We emphasize that all ingredients used in the present analysis have been renormalized at $\mu = 4.3$ GeV; therefore, it is understood that all non-RGI results obtained, such as the $m^2(q)$ and the value of α_s employed, are valid for this particular choice of μ. It would certainly be important to establish the response and overall stability of the mass equation under changes in the value of μ. Even though we

will not pursue this issue any further here, we outline the general method that one should adopt [113]; the basic steps may be summarized as follows: (a) In general, dimensionless quantities, $f(k)$, such as $\mathcal{C}_3(k)$ and $\mathcal{C}_4(k)$, whose form is computed (or assumed) at a scale μ_1, are rescaled to a different point μ_2 according to $f(k,\mu_2) = f(k,\mu_1)/f(\mu_2,\mu_1)$. On the other hand, the gluon propagator corresponding to the lattice result renormalized at μ_2 is obtained from the corresponding result at μ_1 through $\Delta(k,\mu_2) = \Delta(k,\mu_1)/\mu_2^2\Delta(\mu_2,\mu_1)$, (b) The curves of $\mathcal{C}_3(k,\mu_2)$ and $\mathcal{C}_4(k,\mu_2)$ are to be substituted into the mass equation, and the new value of $\alpha_s = \alpha_s(\mu_2)$ must be determined, such that the resulting $m^2(0,\mu_2) = \Delta^{-1}(0,\mu_2)$. (c) The repetition of these steps for a set of $\{\mu_i\}$ will essentially furnish the evolution of α_s that is required by the gluon mass equation; this curve, in turn, must be compared with the evolution of α_s expected on general grounds, and the level of agreement established.

As already mentioned, the kinetic term $J(q)$ of the gluon propagator satisfies its own dynamical equation, which, due to the technical complexities associated with several of its ingredients, has not been presented in the literature. However, recent progress accomplished in various fronts, and especially our firmer knowledge on the behavior of the three-gluon vertex, seems to bring this task well within our reach. In fact, it would be clearly desirable to eventually solve the *coupled system* of equations for $m^2(q)$ and $J(q)$, and establish how closely the lattice results for both the gluon propagator and the three-gluon vertex may be reproduced. Calculations in that directions are already in progress, and we hope to present new results in the near future.

[1] C. D. Roberts and A. G. Williams, Prog. Part. Nucl. Phys. **33**, 477 (1994).

[2] R. Alkofer and L. von Smekal, Phys. Rep. **353**, 281 (2001).

[3] P. Maris and C. D. Roberts, Int. J. Mod. Phys. E **12**, 297 (2003).

[4] J. Greensite, Prog. Part. Nucl. Phys. **51**, 1 (2003).

[5] C. S. Fischer, J. Phys. G **32**, R253 (2006).

[6] J. M. Pawlowski, Ann. Phys. (Amsterdam) **322**, 2831 (2007).

[7] D. Binosi and J. Papavassiliou, Phys. Rep. **479**, 1 (2009).

[8] P. Boucaud, J. P. Leroy, A. L. Yaouanc, J. Micheli, O. Pene, and J. Rodriguez-Quintero, Few-Body Syst. **53**, 387 (2012).

[9] N. Vandersickel and D. Zwanziger, Phys. Rep. **520**, 175 (2012).

[10] A. Maas, Phys. Rep. **524**, 203 (2013).

[11] I. C. Cloet and C. D. Roberts, Prog. Part. Nucl. Phys. **77**, 1 (2014).

[12] C. A. Meyer and E. S. Swanson, Prog. Part. Nucl. Phys. **82**, 21 (2015).

[13] K.-I. Kondo, S. Kato, A. Shibata, and T. Shinohara, Phys. Rep. **579**, 1 (2015).

[14] A. C. Aguilar, D. Binosi, and J. Papavassiliou, Front. Phys. (Beijing) **11**, 111203 (2016).

[15] G. Eichmann, H. Sanchis-Alepuz, R. Williams, R. Alkofer, and C. S. Fischer, Prog. Part. Nucl. Phys. **91**, 1 (2016).

[16] A. K. Cyrol, M. Mitter, J. M. Pawlowski, and N. Strodthoff, Phys. Rev. D **97**, 054006 (2018).

[17] M. Q. Huber, arXiv:1808.05227.

[18] J. M. Cornwall, Phys. Rev. D **26**, 1453 (1982).

[19] C. W. Bernard, Phys. Lett. **108B**, 431 (1982).

[20] C. W. Bernard, Nucl. Phys. **B219**, 341 (1983).

[21] J. F. Donoghue, Phys. Rev. D **29**, 2559 (1984).

[22] K. G. Wilson, T. S. Walhout, A. Harindranath, W.-M. Zhang, R. J. Perry, and S. D. Glazek, Phys. Rev. D **49**, 6720 (1994).

[23] O. Philipsen, Nucl. Phys. **B628**, 167 (2002).

[24] A. C. Aguilar, A. A. Natale, and P. S. R. da Silva, Phys. Rev. Lett. **90**, 152001 (2003).

[25] A. Cucchieri and T. Mendes, Proc. Sci., LAT2007 (**2007**) 297 [arXiv:0710.0412].

[26] A. Cucchieri and T. Mendes, Phys. Rev. Lett. **100**, 241601 (2008).

[27] A. Cucchieri and T. Mendes, Phys. Rev. D **81**, 016005 (2010).

[28] A. Cucchieri, T. Mendes, and E. M. Santos, Phys. Rev. Lett. **103**, 141602 (2009).

[29] I. L. Bogolubsky, E. M. Ilgenfritz, M. Muller-Preussker, and A. Sternbeck, Proc. Sci., LATTICE2007 (**2007**) 290 [arXiv:0710.1968].

[30] P. O. Bowman, U. M. Heller, D. B. Leinweber, M. B. Parappilly, A. Sternbeck, L. von Smekal, A. G. Williams, and J. Zhang, Phys. Rev. D **76**, 094505 (2007).

[31] I. Bogolubsky, E. Ilgenfritz, M. Muller-Preussker, and A. Sternbeck, Phys. Lett. B **676**, 69 (2009).

[32] O. Oliveira and P. Silva, Proc. Sci., LAT2009 (**2009**) 226 [arXiv:0910.2897].

[33] A. Ayala, A. Bashir, D. Binosi, M. Cristoforetti, and J. Rodriguez-Quintero, Phys. Rev. D **86**, 074512 (2012).

[34] P. Bicudo, D. Binosi, N. Cardoso, O. Oliveira, and P. J. Silva, Phys. Rev. D **92**, 114514 (2015).

[35] A. C. Aguilar and A. A. Natale, J. High Energy Phys. 08 (2004) 057.

[36] A. C. Aguilar and J. Papavassiliou, J. High Energy Phys. 12 (2006) 012.

[37] J. Braun, H. Gies, and J. M. Pawlowski, Phys. Lett. B **684**, 262 (2010).

[38] D. Epple, H. Reinhardt, W. Schleifenbaum, and A. Szczepaniak, Phys. Rev. D **77**, 085007 (2008).

[39] A. C. Aguilar, D. Binosi, and J. Papavassiliou, Phys. Rev. D **78**, 025010 (2008).

[40] C. S. Fischer, A. Maas, and J. M. Pawlowski, Ann. Phys. (Amsterdam) **324**, 2408 (2009).

[41] Ph. Boucaud, J. P. Leroy, A. Le Yaouanc, J. Micheli, O. Pène, and J. Rodríguez-Quintero, J. High Energy Phys. 06 (2008) 099.

[42] D. Dudal, J. A. Gracey, S. P. Sorella, N. Vandersickel, and H. Verschelde, Phys. Rev. D **78**, 065047 (2008).

[43] J. Rodriguez-Quintero, J. High Energy Phys. 01 (2011) 105.

[44] D. R. Campagnari and H. Reinhardt, Phys. Rev. D **82**, 105021 (2010).

[45] M. Tissier and N. Wschebor, Phys. Rev. D **82**, 101701 (2010).

[46] M. Pennington and D. Wilson, Phys. Rev. D **84**, 119901 (2011).

[47] J. Serreau and M. Tissier, Phys. Lett. B **712**, 97 (2012).

[48] L. Fister and J. M. Pawlowski, Phys. Rev. D **88**, 045010 (2013).

[49] D. Binosi, L. Chang, J. Papavassiliou, and C. D. Roberts, Phys. Lett. B **742**, 183 (2015).

[50] A. K. Cyrol, M. Q. Huber, and L. von Smekal, Eur. Phys. J. C **75**, 102 (2015).

[51] J. Meyers and E. S. Swanson, Phys. Rev. D **90**, 045037 (2014).

[52] F. Siringo, Nucl. Phys. **B907**, 572 (2016).

[53] A. C. Aguilar, D. Binosi, and J. Papavassiliou, Phys. Rev. D **95**, 034017 (2017).

[54] S. D. Glazek, M. Gómez-Rocha, J. More, and K. Serafin, Phys. Lett. B **773**, 172 (2017).

[55] A. K. Cyrol, J. M. Pawlowski, A. Rothkopf, and N. Wink, SciPost Phys. **5**, 065 (2018).

[56] J. S. Schwinger, Phys. Rev. **125**, 397 (1962).

[57] J. S. Schwinger, Phys. Rev. **128**, 2425 (1962).

[58] J. M. Cornwall and J. Papavassiliou, Phys. Rev. D **40**, 3474 (1989).

[59] A. Pilaftsis, Nucl. Phys. **B487**, 467 (1997).

[60] B. S. DeWitt, Phys. Rev. **162**, 1195 (1967).

[61] J. Honerkamp, Nucl. Phys. **B48**, 269 (1972).

[62] R. E. Kallosh, Nucl. Phys. **B78**, 293 (1974).

[63] H. Kluberg-Stern and J. B. Zuber, Phys. Rev. D **12**, 482 (1975).

[64] L. F. Abbott, Nucl. Phys. **B185**, 189 (1981).

[65] D. Binosi and J. Papavassiliou, Phys. Rev. D **77**, 061702 (2008).

[66] D. Binosi, D. Ibañez, and J. Papavassiliou, Phys. Rev. D **86**, 085033 (2012).

[67] A. C. Aguilar, D. Binosi, and J. Papavassiliou, Phys. Rev. D **89**, 085032 (2014).

[68] A. C. Aguilar, D. Binosi, D. Ibañez, and J. Papavassiliou, Phys. Rev. D **89**, 085008 (2014).

[69] A. C. Aguilar, M. N. Ferreira, C. T. Figueiredo, and J. Papavassiliou, Phys. Rev. D **99**, 094010 (2019).

[70] A. Cucchieri, A. Maas, and T. Mendes, Phys. Rev. D **74**, 014503 (2006).

[71] A. Cucchieri, A. Maas, and T. Mendes, Phys. Rev. D **77**, 094510 (2008).

[72] M. Q. Huber and L. von Smekal, J. High Energy Phys. 04 (2013) 149.

[73] M. Pelaez, M. Tissier, and N. Wschebor, Phys. Rev. D **88**, 125003 (2013).

[74] A. Blum, M. Q. Huber, M. Mitter, and L. von Smekal, Phys. Rev. D **89**, 061703 (2014).

[75] G. Eichmann, R. Williams, R. Alkofer, and M. Vujinovic, Phys. Rev. D **89**, 105014 (2014).

[76] M. Vujinovic, R. Alkofer, G. Eichmann, and R. Williams, Acta Phys. Pol. B Proc. Suppl. **7**, 607 (2014).

[77] A. Athenodorou, D. Binosi, P. Boucaud, F. De Soto, J. Papavassiliou, J. Rodriguez-Quintero, and S. Zafeiropoulos, Phys. Lett. B **761**, 444 (2016).

[78] A. G. Duarte, O. Oliveira, and P. J. Silva, Phys. Rev. D **94**, 074502 (2016).

[79] P. Boucaud, F. De Soto, J. Rodriguez-Quintero, and S. Zafeiropoulos, Phys. Rev. D **95**, 114503 (2017).

[80] C. S. Fischer and R. Alkofer, Phys. Rev. D **67**, 094020 (2003).

[81] A. C. Aguilar and J. Papavassiliou, Phys. Rev. D **83**, 014013 (2011).

[82] A. C. Aguilar, J. C. Cardona, M. N. Ferreira, and J. Papavassiliou, Phys. Rev. D **98**, 014002 (2018).

[83] D. Binosi and J. Papavassiliou, J. High Energy Phys. 11 (2008) 063.

[84] P. A. Grassi, T. Hurth, and M. Steinhauser, Ann. Phys. (Amsterdam) **288**, 197 (2001).

[85] D. Binosi and J. Papavassiliou, Phys. Rev. D **66**, 025024 (2002).

[86] A. C. Aguilar, D. Binosi, J. Papavassiliou, and J. Rodriguez-Quintero, Phys. Rev. D **80**, 085018 (2009).

[87] A. C. Aguilar, D. Ibanez, V. Mathieu, and J. Papavassiliou, Phys. Rev. D **85**, 014018 (2012).

[88] A. C. Aguilar, D. Binosi, C. T. Figueiredo, and J. Papavassiliou, Phys. Rev. D **94**, 045002 (2016).

[89] R. Jackiw and K. Johnson, Phys. Rev. D **8**, 2386 (1973).

[90] J. Smit, Phys. Rev. D **10**, 2473 (1974).

[91] E. Eichten and F. Feinberg, Phys. Rev. D **10**, 3254 (1974).

[92] E. C. Poggio, E. Tomboulis, and S. H. H. Tye, Phys. Rev. D **11**, 2839 (1975).

[93] S. Weinberg, Phys. Rev. D **8**, 3497 (1973).

[94] W. Celmaster and R. J. Gonsalves, Phys. Rev. D **20**, 1420 (1979).

[95] D. Binosi, C. Mezrag, J. Papavassiliou, C. D. Roberts, and J. Rodriguez-Quintero, Phys. Rev. D **96**, 054026 (2017).

[96] J. C. R. Bloch, Phys. Rev. D **64**, 116011 (2001).
[97] J. C. R. Bloch, Phys. Rev. D **66**, 034032 (2002).
[98] D. Binosi, L. Chang, J. Papavassiliou, S.-X. Qin, and C. D. Roberts, Phys. Rev. D **93**, 096010 (2016).
[99] J. S. Ball and T.-W. Chiu, Phys. Rev. D **22**, 2542 (1980).
[100] J. D. Bjorken and S. D. Drell, *Relativistic Quantum Fields*, International Series in Pure and Applied Physics (McGraw-Hill, New York, 1965), ISBN 0070054940.
[101] M. E. Carrington, Phys. Rev. D **87**, 045011 (2013).
[102] R. Williams, C. S. Fischer, and W. Heupel, Phys. Rev. D **93**, 034026 (2016).
[103] N. Mueller and J. M. Pawlowski, Phys. Rev. D **91**, 116010 (2015).
[104] P. Boucaud, F. De Soto, J. Leroy, A. Le Yaouanc, J. Micheli, O. Pène, and J. Rodríguez-Quintero, Phys. Rev. D **79**, 014508 (2009).

[105] P. A. Grassi, T. Hurth, and A. Quadri, Phys. Rev. D **70**, 105014 (2004).
[106] J. A. Gracey, Phys. Rev. D **90**, 025011 (2014).
[107] A. C. Aguilar, M. N. Ferreira, C. T. Figueiredo, and J. Papavassiliou, Phys. Rev. D **99**, 034026 (2019).
[108] D. Binosi, D. Ibañez, and J. Papavassiliou, J. High Energy Phys. 09 (2014) 059.
[109] A. K. Cyrol, L. Fister, M. Mitter, J. M. Pawlowski, and N. Strodthoff, Phys. Rev. D **94**, 054005 (2016).
[110] J. A. Gracey, H. Kißler, and D. Kreimer, Phys. Rev. D **100**, 085001 (2019).
[111] D. Binosi and J. Papavassiliou, Phys. Rev. D **97**, 054029 (2018).
[112] J. S. Ball and T.-W. Chiu, Phys. Rev. D **22**, 2550 (1980).
[113] A. C. Aguilar, D. Binosi, and J. Papavassiliou, J. High Energy Phys. 07 (2010) 002.